

Non-Unitary Quantum Machine Learning

Jamie Heredge^{1*}, Maxwell West¹, Lloyd Hollenberg¹ and Martin Sevier¹

¹School of Physics, University of Melbourne, Parkville, VIC 3010, Australia.

*Corresponding author(s). E-mail(s): heredgej@student.unimelb.edu.au;
Contributing authors: westm2@student.unimelb.edu.au; lloydch@unimelb.edu.au;
martines@unimelb.edu.au;

Abstract

We introduce several novel probabilistic quantum algorithms that overcome the normal unitary restrictions in quantum machine learning by leveraging the Linear Combination of Unitaries (LCU) method. Among our contributions are quantum native implementations of Residual Networks (ResNet); demonstrating a path to avoiding barren plateaus while maintaining the complexity of models that are hard to simulate classically. Furthermore, by generalising to allow control of the strength of residual connections, we show that the lower bound of the LCU success probability can be set to any arbitrary desired value. We also implement a quantum analogue of average pooling layers from convolutional networks. Our empirical analysis demonstrates that the LCU success probability remains stable for the MNIST database, unlocking a potential quadratic advantage in terms of image size compared to classical techniques. Finally, we propose a general framework for irreducible subspace projections for quantum encoded data. Using this, we demonstrate a novel rotationally invariant encoding for point cloud data via Schur-Weyl duality. We also show how this framework can be used to parameterise and control the amount of symmetry in an encoding; demonstrating improved classification performance for partially permutation invariant encoded point cloud data when compared to non-invariant or fully permutation invariant encodings. These new general algorithmic frameworks are all constructed under the same LCU method, suggesting that even more novel algorithms could be achieved by utilising the LCU technique.

Keywords: Quantum Machine Learning, Residual Networks, Quantum ResNet, Encoding Methods, 3D Computer Vision, Quantum Convolutional Neural Networks, Geometric Quantum Machine Learning, Point Cloud Data, Non-unitary Quantum Machine Learning

1 Introduction

Quantum computing is an emerging technology with the potential to solve certain problems far more efficiently than classical techniques [1–3]. The search for useful applications of quantum computers within the domain of machine learning is of particular importance given the significant impact classical machine learning has had on many fields and industries in recent years [4–6]. Various quantum machine learning algorithms have been proposed, with some of the most

common examples attempting to recreate a quantum analogue of the classical neural network [7, 8]. However, the inherently unitary operations of quantum algorithms impose significant limitations, as they restrict the implementation of non-unitary operations that are essential in many classical machine learning models. To address this issue, we explore the Linear Combination of Unitaries (LCU) method [9, 10], a technique that employs ancilla qubits to probabilistically implement a linear combination of unitary

operations, which therefore permits the implementation of non-unitary operations in quantum circuits. This unlocks the possibility of implementing non-unitary operations within quantum machine learning (QML) applications. We utilise this to present several novel applications of the LCU method with various advantages in the field of quantum machine learning.

In Section 2 we adapt the classical residual learning framework to quantum variational circuits, facilitating a quantum native implementation of Residual Networks (ResNet) [11, 12]. We show that this quantum ResNet may provide a method of avoiding barren plateaus in Variational Quantum Circuit (VQC) models while also retaining complexity in the models such that they are overall difficult to simulate classically. Furthermore, we show that by including terms that parameterise the strength of the residual connections, it is possible to increase the lower bound of the probability of success of the LCU procedure to any desired value. This helps to overcome one of the main challenges of LCU methods, the fact that they have a fixed probability of success each time they are implemented.

In Section 3 we implement a quantum analogue of average pooling operations from convolutional neural networks (CNN) [13–15] by using the LCU method, unlocking a new technique for future use in quantum convolutional neural networks. We find that the LCU probability of success will equal 1 in the case where all pixels are of the same colour and will decrease when pixels in the local pooling window of dimension $D \times D$ become more diverse. For real-world images, we provide the intuition that the probability remains relatively stable since most pixels are similar locally, except at the edges of subjects in the image. This intuition is supported by empirical evidence on $N \times N$ pixel images in the MNIST [16] database, which shows that probability decreases but levels off to a finite value as D increases, and shows no discernible trend when increasing image size N . This potentially offers a quadratic advantage in terms of N compared to classical pooling layers, as quantum parallelism allows the averaging of all N^2 pixels simultaneously.

In Section 4 we present a method for projecting quantum encoded data to any combination of irreducible representation subspaces of a finite group, presenting a general framework for implementing full or partial symmetries in the encoding step of quantum machine learning models. These techniques are intended to reduce the effective dimension of quantum encoded data in an effort to improve generalisation performance, which has been reported to decline as the number of qubits and hence the dimension of the encoded quantum states increases [17]. We show that this technique can recreate previous work on permutation invariant encodings for point cloud data

[18] as a special case. Furthermore, we implement a novel rotationally invariant encoding for point cloud data using the new technique by leveraging Schur-Weyl duality. This results in an encoded quantum state for point cloud data that is invariant if classical input point cloud data is rotated in 3-dimensional space, hence strongly enforcing rotation invariance on any model that subsequently uses this rotationally invariant input state. We further show that any combination of projections can be implemented at once, allowing certain symmetric subspaces of the data to be amplified or contracted to give increased flexibility over the amount of symmetry in the encoding. We demonstrate that intermediate levels of permutation symmetry for point cloud encoded data leads to an improved classification performance when compared to a non-symmetric or a fully permutation symmetric encoding.

These implementations illustrate the ability of the LCU method to benefit the field of QML and a summary of these contributions is provided in Table 1. This work covers three different algorithmic frameworks that all utilise the same LCU method in their construction which are located in self-contained sections which may be read in any order:

- **Quantum Native ResNet**
is detailed in Section 2
- **Quantum Native Average Pooling**
is detailed in Section 3
- **Irreducible Representation Projections**
are detailed in Section 4

The remainder of this introductory section will introduce these three frameworks, followed by a summary of the LCU method used in their constructions.

1.1 Quantum Native ResNet

A common issue in the training of variational quantum circuit (VQC) models is the issue of barren plateaus leading to vanishing gradients. Classical Residual Networks (ResNet) have profoundly impacted deep learning by enabling the training of extremely deep neural networks through the introduction of skip connections that mitigate the vanishing gradient problem [11, 12]. This suggests that the implementation of Residual Networks within a quantum variational model could provide a significant advancement in quantum machine learning if they could similarly be utilised to avoid the problem of barren plateaus inherent in many VQC models. This line of reasoning was suggested in a recent review of barren plateaus [19] with the caveat that the no-cloning theorem may make residual and skipped connections difficult to achieve in quantum circuits. In this work, we shall show a probabilistic

Table 1 Summary of the algorithms introduced in this work using the LCU framework. G is a finite compact group. $|\psi_r\rangle$ is the portion of a state $|\psi\rangle$ that occupies the subspace of the irreducible representation r , with $|\psi_{\text{rot}}\rangle$ meaning the portion of $|\psi\rangle$ that is in the rotationally invariant subspace. Note that $\langle\psi_r|\psi_r\rangle$ is not necessarily equal to 1, as the condition is $\langle\psi|\psi\rangle = \sum_r \langle\psi_r|\psi_r\rangle = 1$. The parameters a_r can be chosen by the user subject to normalisation constraints. In average pooling we use a pooling window of dimension $D \times D$ pixels. L is the number of layers in the quantum ResNet. $\beta_l \in [0, 1]$, $\beta_l \in \mathbb{R}$ parameterise the strength of the skipped connections in the quantum ResNet and can be freely adjusted. Throughout this work $\log \equiv \log_2$ is the logarithmic function in base 2.

Algorithm	Motivation	Ancilla Qubits	Success Probability	Section
Quantum ResNet Residual Layers	Potentially avoids barren plateaus in non-simulatable models	$\mathcal{O}(L)$	$[\prod_l (1 - 4\beta_l(1 - \beta_l)), 1]$	Sec 2
Average Pooling	Potential quadratic speedup in N over averaging classically	$\mathcal{O}(\log(D))$	Shown for MNIST in Fig 7 and Fig 8.	Sec 3
Irreducible Subspace Projections	Can freely enforce and parameterise symmetry of a quantum encoded state	$\mathcal{O}(\log(G))$	$\sum_r a_r ^2 \langle\psi_r \psi_r\rangle$	Sec 4
Rotationally Invariant Encoding	Encoding respects rotational invariance of point cloud data	$\mathcal{O}(\log(G))$	$\langle\psi_{\text{rot}} \psi_{\text{rot}}\rangle$	Sec 4.3.2

implementation of a quantum native ResNet that does not require cloning states and could show promise against barren plateaus in VQC models.

There has been active interest in building quantum ResNet type algorithms in the literature, with a primary focus being on quantum-classical hybrid models, that use the powerful modern architecture of classical ResNet models, while including quantum machine learning subroutines to produce a hybrid algorithm [20–22]. There have also been proposals to implement quantum residual connections by utilising several quantum neural network models in series with residual connections between them [23]. A native VQC implementation of a quantum ResNet algorithm has previously been introduced in [24], in which skipped connections are possible in a VQC model if the implemented variational layers are restricted to be of the form of a unitary circuit followed by a product Pauli encoding, followed by the unitary circuit conjugate. This implements the quantum ResNet natively on a quantum device; however, as the authors note, this does not cover any general unitary variational layer $W_i(\theta_i)$, since implementing residual connections for a general $W_i(\theta_i)$ would not be a unitary process overall and was therefore not considered in this approach. A common theme explored in these previous works was utilising the effectiveness of classical ResNet models in tackling the vanishing gradients problem of deep neural networks and applying this reasoning in a quantum setting to the problem of barren plateaus.

Applying residual connections in a quantum setting corresponds to operating on a state $|\psi_{l-1}\rangle$ to produce

$$|\psi_l\rangle = W_l(\theta_l)|\psi_{l-1}\rangle + |\psi_{l-1}\rangle, \quad (1)$$

whereby a portion of the previous state $|\psi_{l-1}\rangle$ is able to skip the variational operator $W_l(\theta_l)$ in that layer. This allows the overall model cost function to retain terms that have only passed through one variational layer, corresponding to very short circuits, while still providing terms that have been passed through all layers and hence potentially very deep circuits. The operator which would result in this would be of the form

$$A_l = W_l(\theta_l) + I, \quad (2)$$

which in general is not a unitary operator. The key challenge therefore in implementing a quantum native ResNet analogue is that it would require implementation of non-unitary operators, something that becomes possible with the LCU framework. In this work, we translate the ResNet architecture to a quantum setting by applying residual connection with the LCU framework to facilitate the flow of quantum information across deeper or more complex quantum circuits, while allowing the strength of the residual connection to be chosen freely. This introduces a potential new class of VQC ResNet models which could provide possible protection against barren plateaus in complex VQC models.

1.2 Average Pooling Layers

Classical Convolution Neural Networks (CNN) are of significant importance to machine learning, mainly due to their structured manner of handling image and video data [13–15]. Inspiration from these models has led to the development of quantum analogues. Quantum convolution neural networks have been previously proposed [25, 26] to classify quantum states with certain symmetry-protected topological phases and to

classify image datasets [27, 28]. In these models variational circuits are used during convolutional layers followed by further variational circuits and measurements in the pooling layer to perform dimensionality reduction, such that the operations are performed in a manner that respects certain symmetries of the data. Significant benefits of these models, such as avoiding barren plateaus [29], have been identified. Quantum-classical hybrid techniques have also been developed that utilise classical convolution neural network architectures alongside quantum models [30].

The implementation we present here differs in that we focus entirely on implementing a subroutine of classical CNN models, the average pooling layer, for amplitude encoded image data. We consider the subroutine where a pooling window of size $D \times D$ passes over the image and outputs the average of all pixels found within the pooling window. We show that this can be implemented natively on a quantum circuit by utilising the LCU method and further that this potentially leads to quadratic speedup in N , for images of dimension $N \times N$, over performing the subroutine’s classical implementation due to quantum parallelism. This demonstrates the possible utility of the LCU method, while providing a potentially advantageous subroutine for future quantum convolutional neural network models.

1.3 Irreducible Representation Subspace Symmetry Projections

A known issue in Quantum Machine Learning (QML) is that as the number of qubits increases there is a decrease in the generalisation performance of algorithms [17]. A common empirical explanation of this is that the exponentially large Hilbert space leads to an overly expressive feature encoding where overtraining on the data becomes commonplace. Without an accompanied exponential increase in the training data, this leads to an overall reduction in the performance in the validation data set. A possible solution to the issue of overtraining is to reduce the expressibility of the encoding. Examples of techniques that have attempted this range from projecting kernels to a lower-dimensional space [31] and approaches that are capable of encoding inductive biases directly into quantum states [32]. Furthermore, geometric QML techniques have studied methods for creating variational circuits that are equivariant with respect to data symmetries [33–37] in similar attempts to reduce the expressibility of QML models. We instead focus on implementing symmetries directly into the quantum encoded data, which is a stricter implementation of symmetry, meaning our procedure is agnostic to the trainable classification procedure.

In previous work a quantum encoding was proposed using permutation symmetry, which led to a reduction in the dimensionality of the encoding and improved classification performance [18]. This was discussed in the context of point cloud data (unordered collection of points in 3 dimensions that collectively represent an image), where each point cloud X consists of n points and each point \mathbf{p}_i is a 3-dimensional vector. As points do not have intrinsic ordering, the ordering of the points as they are input into a classification algorithm should ideally have no effect on the outcome. Therefore, the point cloud data naturally has point ordering permutation invariance. In general, a machine learning classifier f , could return a different result depending on the order of the points, that is, $f(\mathbf{p}_1, \mathbf{p}_2) \neq f(\mathbf{p}_2, \mathbf{p}_1)$, unless it has been specifically constructed to respect the permutation symmetry. The permutation invariant encoding [18] acts by creating an equal quantum superposition of all permutations of the data. In the two-state case, given two points $\mathbf{p}_1, \mathbf{p}_2$ encoded into the quantum state $|\mathbf{p}_1\rangle \otimes |\mathbf{p}_2\rangle$ this would correspond to preparing the permutation invariant state

$$|X_s\rangle = \frac{1}{\sqrt{2}}(|\mathbf{p}_1\rangle|\mathbf{p}_2\rangle + |\mathbf{p}_2\rangle|\mathbf{p}_1\rangle), \quad (3)$$

However, it has been shown that the permutation invariant state preparation procedure

$$|\mathbf{p}_1\rangle|\mathbf{p}_2\rangle \Rightarrow \frac{1}{\sqrt{2}}(|\mathbf{p}_1\rangle|\mathbf{p}_2\rangle + |\mathbf{p}_2\rangle|\mathbf{p}_1\rangle), \quad (4)$$

cannot be implemented via a unitary operation [38]. However, this process can be implemented in a probabilistic manner using ancilla qubits [39]. This was shown to lead to improved classification performance for point cloud image classification [18].

In this work, we demonstrate a generalisation of this technique that allows projections to any irreducible representation subspace of a finite group. Unlike previous works [18], this means that we are no longer restricted to the symmetric subspace or the permutation group S_n . Furthermore, our technique allows for linear combinations of projections to any irreducible representation subspaces.

Utilising this framework, we demonstrate a rotationally invariant encoding for point cloud data as an example use case. This encoding produces the same quantum encoded state each time, even if the data input point cloud is rotated by any amount in 3-dimensions. We show that this is achieved both theoretically and numerically. This is a highly desirable property of the model as point cloud data naturally has rotational symmetry. Especially in applications such as computer vision for autonomous vehicles it is

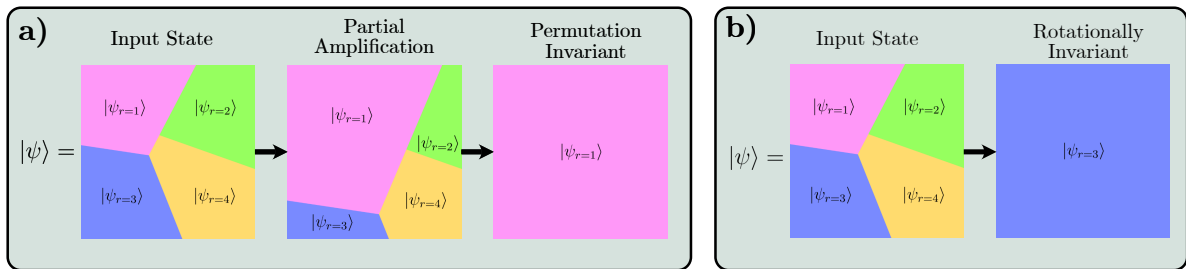


Fig. 1 Visual representation of the irreducible subspace projection of a quantum state. The input state $|\psi\rangle$ has components in each irreducible representation subspace denoted by $|\psi_r\rangle$. a) The component of $|\psi\rangle$ in the subspaces can be partially amplified to any desired ratio between the subspace components. Controlling the amplification of the permutation symmetric subspace $|\psi_{r=1}\rangle$ for point cloud data is the focus of Section 4.4. The state can also be fully projected to $|\psi_{r=1}\rangle$ which for the permutation group S_n would correspond to a fully permutation invariant state. Permutation invariant encodings have been the subject of previous work [18] and are reviewed within our new framework in Section 4.3.1. b) The input state $|\psi\rangle$ is fully projected to $|\psi_{r=3}\rangle$ within the $r = 3$ irreducible subspace. In Section 4.3.2 we show that this corresponds to creating rotationally invariant encodings of point cloud data.

of utmost importance that subjects in the image, such as pedestrians, are correctly identified regardless of the angle from which they are being viewed. Previous work has focused on implementing rotational and permutation symmetry into models for point cloud data [40], which did so by implementing an equivariant variational model. We highlight that our work does not use equivariant variational models, but projects quantum input states to a rotationally invariant subspace, hence strictly enforcing rotational invariance into any model for which this input encoded state is passed, as we effectively delete all information of the state which is not rotationally invariant.

The permutation and rotationally invariant encodings mentioned previously succeed in reducing the dimension of the encoding, but we note that this reduction may indeed be too drastic, which could lead to classically simulatable approaches or simply delete too much information about the input state, hindering the model performance. We therefore show how our new framework allows for linear combinations of projections that can be utilised to introduce parameterised symmetry subspace amplification. In this model, the amount of symmetry can be continuously adjusted using a hyperparameter α . We show that by implementing an intermediate amount of permutation symmetry for point cloud data classification, it is possible to gain higher accuracy scores than using either non-invariant encodings or the fully permutation invariant encodings suggested in previous work [18]. A visualisation of these applications is shown in Figure 1.

1.4 Linear Combinations of Unitaries Method

All results in this paper are specific cases of the LCU method described in this section. Let us define the general framework of how the LCU method works in a quantum circuit as detailed in [9, 10]. An insightful tutorial on the LCU method can also be found at [41]. The LCU procedure allows the implementation of any operator A that is itself a linear combination of N unitary operators $U_j \in SU(2^n)$. The operator A acts on a target state that is contained in an n qubit target register. The target state is denoted $|\psi\rangle \in (\mathbb{C}^2)^{\otimes n}$. We can define the operator A acting on $|\psi\rangle$ as

$$A|\psi\rangle = \frac{1}{\Omega'} \sum_{j=1}^N \alpha_j U_j |\psi\rangle, \quad (5)$$

where for simplicity $\alpha_j \geq 0$, $\alpha_j \in \mathbb{R}$ and any negative sign or complex phase can be absorbed into the unitary $U_j \in SU(2^n)$ and Ω' is a normalisation constant for the final target state.

In order to implement this, we need to define an ancilla preparation operator P_{PREP} which prepares the k ancilla qubits, that are initially in a basis state $|b_1\rangle$, into the following state

$$P_{\text{PREP}}|b_1\rangle = \frac{1}{\sqrt{\Omega}} \sum_{j=1}^N \sqrt{\alpha_j} |b_j\rangle, \quad (6)$$

where $\Omega = \sum_{j=1}^N \alpha_j$ is a normalisation constant for the ancilla state and $\{|b_j\rangle\} \in (\mathbb{C}^2)^{\otimes k}$ are basis states of the 2^k dimensional Hilbert space for the k qubit ancilla register denoted by $\mathcal{H} = (\mathbb{C}^2)^{\otimes k}$, which can be taken to be the computational basis states. The

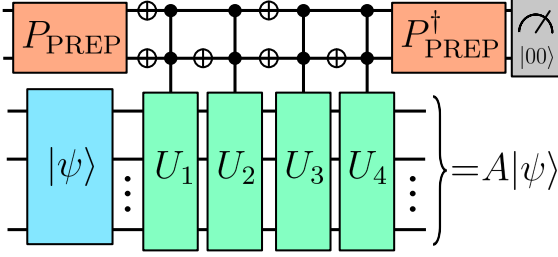


Fig. 2 Visual representation of the LCU procedure to implement $A|\psi\rangle = \frac{1}{\Omega'}(\alpha_1 U_1 + \alpha_1 U_2 + \alpha_1 U_3 + \alpha_1 U_4)|\psi\rangle$. The upper two qubits are the ancilla qubits initially prepared by the P_{PREP} operator to be in the state $P_{\text{PREP}}|b_1\rangle = \frac{1}{\sqrt{\Omega}} \sum_{j=1}^N \sqrt{\alpha_j} |b_j\rangle$. Note that in this case $|b_1\rangle \equiv |00\rangle$ and will implement U_1 . $|b_2\rangle \equiv |01\rangle$ and will implement U_2 . $|b_3\rangle \equiv |10\rangle$ and will implement U_3 . $|b_4\rangle \equiv |11\rangle$ and will implement U_4 . The inverse preparation P_{PREP}^\dagger is then applied and the ancillas are measured. If the ancillas are measured to be in the state $|b_1\rangle \equiv |00\rangle$ then A is successfully implemented on the target state $|\psi\rangle$. This example demonstrates how multi-control unitary gates can be implemented in practice which are controlled by the ancilla qubits and applied to the target register containing $|\psi\rangle$.

operator itself can be explicitly written as

$$P_{\text{PREP}} = \frac{1}{\sqrt{\Omega}} \sum_{j=1}^N \sqrt{\alpha_j} |b_j\rangle \langle b_1| + \sum_{i=2}^{2^k} \sum_{j=1}^{2^k} \delta_{i,j} |b_j\rangle \langle b_i|, \quad (7)$$

where any terms $(\dots)\langle b_i|$ for $i \geq 2$ will not be used and hence can be ignored.

After the ancilla qubits are prepared, we then apply a selection operator S_{SELECT} . The selection operator applies the unitary operation $U_j \in SU(2^n)$ to the target register state $|\psi\rangle$ on the condition that the ancilla qubit is in the state $|b_j\rangle$, which can be defined as

$$S_{\text{SELECT}}|b_j\rangle|\psi\rangle = |b_j\rangle U_j |\psi\rangle. \quad (8)$$

If we now combine the preparation and selection operators, we have

$$S_{\text{SELECT}} P_{\text{PREP}} |b_1\rangle |\psi\rangle = \frac{1}{\sqrt{\Omega}} \sum_{j=1}^N \sqrt{\alpha_j} |b_j\rangle U_j |\psi\rangle. \quad (9)$$

The final step consists of applying P_{PREP}^\dagger which is defined as

$$P_{\text{PREP}}^\dagger = \frac{1}{\sqrt{\Omega}} \sum_{j=1}^N \sqrt{\alpha_j} |b_1\rangle \langle b_j| + \sum_{i=2}^{2^k} \sum_{j=1}^{2^k} \delta_{i,j}^* |b_i\rangle \langle b_j|. \quad (10)$$

Applying this to the circuit results in

$$\begin{aligned} & P_{\text{PREP}}^\dagger S_{\text{SELECT}} P_{\text{PREP}} |0\rangle |\psi\rangle \\ &= \frac{1}{\Omega} \sum_{j=1}^N \alpha_j |b_1\rangle U_j |\psi\rangle + \sum_{i=2}^{2^k} (\dots) |b_i\rangle |\psi\rangle, \end{aligned} \quad (11)$$

where $\sum_{i=2}^{2^k} (\dots) |b_i\rangle |\psi\rangle$ collects terms that will be discarded and can therefore be ignored. We now need to measure the ancilla register and discard any results when the ancilla is not measured in the $|b_1\rangle$ state. The probability of measuring the $|b_1\rangle$ state will equal the probability of success of the LCU method π_S which can be written as

$$\pi_S = \left| \frac{1}{\Omega} \sum_{j=1}^N \alpha_j U_j |\psi\rangle \right|^2. \quad (12)$$

Discarding any results in which the ancilla is not measured in the $|b_1\rangle$ state we see that the remaining state will be projected to

$$\langle 0 | P_{\text{PREP}}^\dagger | S_{\text{SELECT}} | P_{\text{PREP}} | 0 \rangle |\psi\rangle = \frac{1}{\Omega'} \sum_{j=1}^N \alpha_j U_j |\psi\rangle, \quad (13)$$

where $\Omega' = \sqrt{\pi_S} \Omega$ is the normalisation constant for the final state, which can then be written as

$$\frac{1}{\Omega'} \sum_{j=1}^N \alpha_j U_j |\psi\rangle = A |\psi\rangle. \quad (14)$$

Hence, the operator A , which is a linear combination of unitaries and hence may itself be non-unitary, has been applied to the state $|\psi\rangle$ [42].

The goal of this work is to demonstrate how the LCU method described above can be used in QML tasks to achieve desirable traits in the model architecture that are not possible in a strict unitary setting. The main results of this work rely on specifying preparation and selection operators, showing that they can be implemented on a quantum device, and then repeating the LCU framework detailed here to prove that they result in the desired non-unitary operation. An example LCU circuit for the implementation of $A|\psi\rangle = \frac{1}{\Omega'}(\alpha_1 U_1 + \alpha_1 U_2 + \alpha_1 U_3 + \alpha_1 U_4)|\psi\rangle$ is shown in Figure 2.

2 Quantum Native ResNet

2.1 Variational Quantum Circuit Model Preliminaries

For a vector of classical input data $\mathbf{x} \in \mathbb{R}^d$ a standard quantum variational circuit model consists of an n qubit encoding circuit $V(\mathbf{x}) \in SU(2^n)$ that encodes the classical data into a quantum state $|\psi_0\rangle \equiv |\phi(\mathbf{x})\rangle = V(\mathbf{x})|0\rangle^{\otimes n}$. This encoded state can also be represented as a density matrix defined by

$$\rho(\mathbf{x}) = V(\mathbf{x})|0\rangle^{\otimes n}\langle 0|^{\otimes n}V(\mathbf{x})^\dagger. \quad (15)$$

Alternatively $|\psi_0\rangle$ and $\rho = |\psi_0\rangle\langle\psi_0|$ could be quantum data in which no encoding process needs to be considered.

The input state $|\psi_0\rangle$ is then passed through L layers of variational quantum circuits $W_l(\boldsymbol{\theta}_l) \in SU(2^n)$ where $\boldsymbol{\theta}_l = (\theta_{l1}, \theta_{l2}, \dots, \theta_{lD_l})$ is a vector of variational parameters that can be adjusted as the model is trained. We can therefore represent the overall variational circuit as

$$W(\boldsymbol{\theta}) = \prod_{l=1}^L W_l(\boldsymbol{\theta}_l), \quad (16)$$

where $\boldsymbol{\theta}$ is a vector containing all variational parameters for all layers such that $\boldsymbol{\theta} = \{\boldsymbol{\theta}_l\}, l \in [1, L]$. Finally, measurement is made of some Hermitian observable O . For simplicity, we will consider a loss function for the model defined as

$$\mathcal{L}_{\boldsymbol{\theta}}(\rho, O) \equiv \langle O \rangle_{\rho, \boldsymbol{\theta}} = \text{Tr}(W(\boldsymbol{\theta})\rho W(\boldsymbol{\theta})^\dagger O), \quad (17)$$

where any insights from this loss function with regards to barren plateaus can often be extended to other, more general loss functions. Training a model consists of variationally adjusting the parameters $\boldsymbol{\theta}$ until the cost function matches some known data labels y to within some acceptable error.

2.2 Quantum ResNet Implementation

The key concept of ResNet [11] is the introduction of residual blocks. Instead of learning a mapping $H(a)$ on some data, the model instead learns some residual function $W(a)$ such that

$$H(a) = a + W(a), \quad (18)$$

where a is the input to the block, $W(a)$ is the learned residual mapping and $H(a)$ is the output of the block.

This means the output a_l of each layer l can be defined by

$$a_l = a_{l-1} + W_l(a_{l-1}, \boldsymbol{\theta}_l), \quad (19)$$

where a_0 is the initial data input. In order to create a quantum version of this framework, we consider the Quantum ResNet [24] that can be defined as

$$|\psi_l\rangle = |\psi_{l-1}\rangle + W_l(\boldsymbol{\theta}_l)|\psi_{l-1}\rangle, \quad (20)$$

where $W_l(\boldsymbol{\theta}_l)$ is the variational unitary for layer l , $|\psi_l\rangle$ is the output of the layer, $|\psi_{l-1}\rangle$ is the input of the layer, and $|\psi_0\rangle$ corresponds to the initial input state. This initial data input state could be quantum data $|\psi_0\rangle$ or it could be a quantum state which encodes classical data $|\psi_0\rangle = |\phi(\mathbf{x})\rangle$, where $\mathbf{x} \in \mathbb{R}^d$ is a d -dimensional classical input data vector encoded into a quantum state through a data encoding circuit $V(\mathbf{x})$ such that $|\phi(\mathbf{x})\rangle = V(\mathbf{x})|0\rangle^{\otimes n}$. Implementation of Quantum ResNet of this form involves applying an operator

$$A_{\text{RES}} = (I + W_l(\boldsymbol{\theta}_l)), \quad (21)$$

to the state $|\psi_{l-1}\rangle$. This presents a problem as the operator is not necessarily unitary in general for all $W_l(\boldsymbol{\theta}_l) \in SU(2^n)$. Therefore, we proceed with implementing it via the LCU method.

To maintain the most general case, and to aid in the probability scaling of the LCU procedure, we shall consider adding some additional control into the magnitude of the skipped connections parameterised for each layer by some amount $\beta_l \in \mathbb{R}$. Therefore the definition of a quantum residual connection we shall use is

$$|\psi_l\rangle = \frac{1}{\Omega'}((1 - \beta_l)|\psi_{l-1}\rangle + \beta_l W_l(\boldsymbol{\theta}_l)|\psi_{l-1}\rangle), \quad (22)$$

where Ω' is a normalisation constant.

This can be encoded with the LCU framework in a quantum circuit by applying the $P_{\text{PREP}}^{(l)}$ single qubit operator to the l -th ancilla qubit denoted by $|0\rangle^{(l)}$ defined by

$$P_{\text{PREP}}^{(l)} = (\sqrt{1 - \beta_l}|0\rangle^{(l)} + \sqrt{\beta_l}|1\rangle^{(l)})\langle 0|^{(l)} + (\dots)\langle 1|^{(l)}, \quad (23)$$

where terms involving $(\dots)\langle 1|^{(l)}$ do not have an effect on the circuit and can be ignored. Hence we can write the action of preparing the l -th ancilla qubit as

$$P_{\text{PREP}}^{(l)}|0\rangle^{(l)} = (\sqrt{1 - \beta_l}|0\rangle^{(l)} + \sqrt{\beta_l}|1\rangle^{(l)}), \quad (24)$$

such that $P_{\text{PREP}}|0\rangle^{\otimes L} = \bigotimes_{l=1}^L P_{\text{PREP}}^{(l)}|0\rangle^{(l)}$ and hence

$$P_{\text{PREP}}|0\rangle^{\otimes L} = \bigotimes_{l=1}^L (\sqrt{1-\beta_l}|0\rangle^{(l)} + \sqrt{\beta_l}|1\rangle^{(l)}), \quad (25)$$

where for simplicity $\beta_l \in \mathbb{R}$. The selection operator is defined to be controlled by the l -th ancilla qubit as

$$S_{\text{SELECT}}^{(l)}|0\rangle^{(l)}|\psi\rangle = |0\rangle^{(l)}|\psi\rangle, \quad (26)$$

$$S_{\text{SELECT}}^{(l)}|1\rangle^{(l)}|\psi\rangle = |1\rangle^{(l)}W_l(\boldsymbol{\theta}_l)|\psi\rangle. \quad (27)$$

We can then define the overall selection operator by specifying the ordering

$$S_{\text{SELECT}} = \prod_{l=1}^L S_{\text{SELECT}}^{(L-l+1)} = S_{\text{SELECT}}^{(L)} \cdots S_{\text{SELECT}}^{(1)}, \quad (28)$$

such that $S_{\text{SELECT}}^{(1)}$ is applied first.

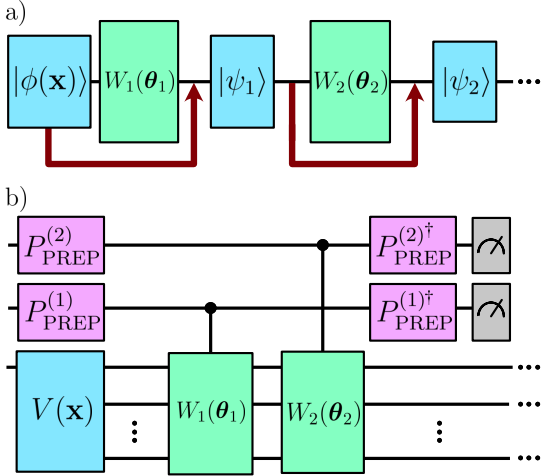


Fig. 3 a) Classical ResNet conceptual illustration in which residual information can be skipped over each layer. b) Quantum ResNet implementation using LCU methods, showing the first two layers only. In this case a quantum analogue of ResNet can be probabilistically implemented using ancilla qubits. The $P_{\text{PREP}}^{(1)}$ prepares the first ancilla qubit into the state $(\sqrt{1-\beta_1}|0\rangle^{(1)} + \sqrt{\beta_1}|1\rangle^{(1)})$; when this ancilla is measured at the end in the $|0\rangle^{(1)}$ state it corresponds to applying the operator $(1-\beta_1)\mathbb{I} + \beta_1 W_1(\boldsymbol{\theta}_1)$ to the initial input state $|\phi(\mathbf{x})\rangle = V(\mathbf{x})|0\rangle^{\otimes n}$. The process is repeated for future layers allowing a portion of the quantum state to skip each layer and be added to the output of the layer.

Theorem 1 (Quantum ResNet) *It is possible to probabilistically implement a Quantum ResNet architecture on a quantum circuit where each layer of the variational circuit permits a residual connection defined as*

$$|\psi_l\rangle = \frac{1}{\Omega'} ((1-\beta_l)|\psi_{l-1}\rangle + \beta_l W_l(\boldsymbol{\theta}_l)|\psi_{l-1}\rangle),$$

where $W_l(\boldsymbol{\theta}_l)$ is the l -th layer of the variational circuit, the constants $\beta_l \in \mathbb{R}$, $\beta_l \in [0, 1]$ can be chosen freely, the input to the layer is the state $|\psi_{l-1}\rangle$ and the output of the layer is the state $|\psi_l\rangle$. The term Ω' is a normalisation constant. The algorithm can be applied for all layers $l \in [1, L]$ simultaneously with a fixed probability of success

$$\pi_S = \prod_{l=1}^L (1 - 2\beta_l(1-\beta_l)(1 - \text{Re}(\langle \psi_{l-1} | W_l(\boldsymbol{\theta}_l) | \psi_{l-1} \rangle))),$$

where $|\psi_0\rangle$ is an initial input state given to the algorithm which can be quantum data, or a quantum state encoded by classical data via an encoding circuit $V(\mathbf{x})$ such that $|\psi_0\rangle = |\phi(\mathbf{x})\rangle = V(\mathbf{x})|0\rangle^{\otimes n}$.

Proof We use the preparation and selection operators defined in Equation 25 and Equation 28, respectively, with the LCU framework as outlined in Section 1.4.

The P_{PREP} operator corresponds to performing single qubit initialisation on L qubits and is clearly implementable on a quantum device. Likewise S_{SELECT} corresponds to a controlled $W_l(\boldsymbol{\theta}_l)$ gate, where $W_l(\boldsymbol{\theta}_l)$ is defined to be unitary, which is controlled by the l -th qubit. As $W_l(\boldsymbol{\theta}_l)$ is unitary, the S_{SELECT} operation is also implementable on a quantum device.

We consider applying the LCU procedure to the first ancilla qubit only. Starting with the first qubit preparation operator

$$\begin{aligned} P_{\text{PREP}}^{(1)}|0\rangle^{\otimes L}|\psi_0\rangle &= (\sqrt{1-\beta_1}|0\rangle^{(1)} + \sqrt{\beta_1}|1\rangle^{(1)}) \bigotimes_{l=2}^L |0\rangle^{(l)}|\psi_0\rangle. \end{aligned} \quad (29)$$

Subsequently, the selection operator which is controlled by the first qubit is applied

$$\begin{aligned} S_{\text{SELECT}}^{(1)}P_{\text{PREP}}^{(1)}|0\rangle^{\otimes L}|\psi_0\rangle &= S_{\text{SELECT}}^{(1)}(\sqrt{1-\beta_1}|0\rangle^{(1)} + \sqrt{\beta_1}|1\rangle^{(1)}) \bigotimes_{l=2}^L |0\rangle^{(l)}|\psi_0\rangle \\ &= \sqrt{1-\beta_1}|0\rangle^{(1)} \bigotimes_{l=2}^L |0\rangle^{(l)}|\psi_0\rangle \\ &\quad + \sqrt{\beta_1}|1\rangle^{(1)} \bigotimes_{l=2}^L |0\rangle^{(l)}W_1(\boldsymbol{\theta}_1)|\psi_0\rangle. \end{aligned} \quad (30)$$

Consider the conjugate preparation operator,

$$(P_{\text{PREP}}^{(1)})^\dagger = |0\rangle^{(1)}(\sqrt{1-\beta_1}\langle 0|^{(1)} + \sqrt{\beta_1}\langle 1|^{(1)}) + |1\rangle^{(1)}(\dots), \quad (31)$$

where $|1\rangle^{(1)}(\dots)$ collects terms that will not be used, as we will require the ancilla to be in the $|0\rangle^{(1)}$ state. Applying this conjugate operator we can write the state as

$$(P_{\text{PREP}}^{(1)})^\dagger S_{\text{SELECT}}^{(1)} P_{\text{PREP}}^{(1)} |0\rangle^{\otimes L} |\psi_0\rangle = |0\rangle^{(1)} \left((1-\beta_1) \bigotimes_{l=2}^L |0\rangle^{(l)} |\psi_0\rangle + \beta_1 \bigotimes_{l=2}^L |0\rangle^{(l)} W_1(\boldsymbol{\theta}_1) |\psi_0\rangle \right) + |1\rangle^{(1)}(\dots), \quad (32)$$

where $|1\rangle^{(1)}(\dots)$ collects terms that will be discarded and can therefore be ignored. The first ancilla qubit is now measured and the result discarded unless it is found to be in the $|0\rangle^{(1)}$ state. The probability of measuring the ancilla in the $|0\rangle^{(1)}$ state will be equal to

$$\begin{aligned} \pi_1 &= |(1-\beta_1)|\psi_0\rangle + \beta_1 W_1(\boldsymbol{\theta}_1)|\psi_0\rangle|^2 \\ &= 1 - 2\beta_1(1-\beta_1)(1 - \text{Re}(\langle \psi_0 | W_1(\boldsymbol{\theta}_1) | \psi_0 \rangle)), \end{aligned} \quad (33)$$

which will depend on the strength of the residual connection parameterised by β_1 as well as the real component of $\langle \psi_0 | W_1(\boldsymbol{\theta}_1) | \psi_0 \rangle$, which will depend on the quantum encoded state $|\psi_0\rangle$ and the variational operator used $W_1(\boldsymbol{\theta}_1)$.

If we succeed in finding the first ancilla in the $|0\rangle^{(1)}$ state, then the target state will now be

$$\begin{aligned} \langle 0|^{(1)} (P_{\text{PREP}}^{(1)})^\dagger S_{\text{SELECT}}^{(1)} P_{\text{PREP}}^{(1)} |0\rangle^{\otimes L} |\psi_0\rangle &= \\ \frac{1}{\sqrt{\pi_1}} \left((1-\beta_1) \bigotimes_{l=2}^L |0\rangle^{(l)} |\psi_0\rangle + \beta_1 \bigotimes_{l=2}^L |0\rangle^{(l)} W_1(\boldsymbol{\theta}_1) |\psi_0\rangle \right), \end{aligned} \quad (34)$$

and hence ignoring the extra ancilla qubits we have

$$|\psi_1\rangle = \frac{1}{\Omega'_1} \left((1-\beta_1)|\psi_0\rangle + \beta_1 W_1(\boldsymbol{\theta}_1)|\psi_0\rangle \right), \quad (35)$$

where $\Omega'_1 = \sqrt{\pi_1}$ is the required normalisation constant. Hence, for layer $l = 1$ we have shown the quantum residual connection defined in Equation 22 is implemented for the original input state $|\psi_0\rangle$.

Assume now that $|\psi_{p-1}\rangle$ is correctly implemented by the procedure and consider the subsequent implementation of $|\psi_p\rangle$. We prepare the p -th ancilla using

$$P_{\text{PREP}}^{(p)} |0\rangle^{\otimes L-p} |\psi_{p-1}\rangle$$

$$= (\sqrt{1-\beta_p}|0\rangle^{(p)} + \sqrt{\beta_p}|1\rangle^{(p)}) \bigotimes_{l=p+1}^L |0\rangle^{(l)} |\psi_{p-1}\rangle. \quad (36)$$

Through the same procedure as previously we see

$$\begin{aligned} S_{\text{SELECT}}^{(p)} P_{\text{PREP}}^{(p)} |0\rangle^{\otimes L-p} |\psi_{p-1}\rangle &= \\ \sqrt{1-\beta_p}|0\rangle^{(p)} \bigotimes_{l=p+1}^L |0\rangle^{(l)} |\psi_{p-1}\rangle &+ \\ \sqrt{\beta_p}|1\rangle^{(p)} \bigotimes_{l=p+1}^L |0\rangle^{(l)} W_p(\boldsymbol{\theta}_p) |\psi_{p-1}\rangle. \end{aligned} \quad (37)$$

Applying the conjugate preparation operator for the p -th qubit which may be written as

$$(P_{\text{PREP}}^{(p)})^\dagger = |0\rangle^{(p)}(\sqrt{1-\beta_p}\langle 0|^{(p)} + \sqrt{\beta_p}\langle 1|^{(p)}) + |1\rangle^{(p)}(\dots), \quad (38)$$

to the ancillas we see that

$$\begin{aligned} (P_{\text{PREP}}^{(p)})^\dagger S_{\text{SELECT}}^{(p)} P_{\text{PREP}}^{(p)} |0\rangle^{\otimes L-p} |\psi_0\rangle &= \\ (1-\beta_p)|0\rangle^{(p)} \bigotimes_{l=p+1}^L |0\rangle^{(l)} |\psi_{p-1}\rangle &+ \\ \beta_p|0\rangle^{(p)} \bigotimes_{l=p+1}^L |0\rangle^{(l)} W_p(\boldsymbol{\theta}_p) |\psi_{p-1}\rangle + |1\rangle^{(p)}(\dots), \end{aligned} \quad (39)$$

where $|1\rangle^{(p)}(\dots)$ collects terms that will end up being discarded and hence can be ignored. Measuring the ancilla qubit we can see that the probability of measuring the p -th qubit in the $|0\rangle^{(p)}$ state is given by

$$\begin{aligned} \pi_p &= |((1-\beta_p)|\psi_{p-1}\rangle + \beta_p W_p(\boldsymbol{\theta}_p)|\psi_{p-1}\rangle)|^2 \\ &= 1 - 2\beta_p(1-\beta_p)(1 - \text{Re}(\langle \psi_{p-1} | W_p(\boldsymbol{\theta}_p) | \psi_{p-1} \rangle)), \end{aligned} \quad (40)$$

Ensuring the process is only continued if the ancilla is in the $|0\rangle^{(p)}$ state we find

$$\begin{aligned} \langle 0|^{(p)} (P_{\text{PREP}}^{(p)})^\dagger S_{\text{SELECT}}^{(p)} P_{\text{PREP}}^{(p)} |0\rangle^{\otimes L-p} |\psi_0\rangle &= \\ \frac{1}{\sqrt{\pi_p}} \left((1-\beta_p) \bigotimes_{l=p+1}^L |0\rangle^{(l)} |\psi_{p-1}\rangle \right. &+ \\ \left. \beta_p \bigotimes_{l=p+1}^L |0\rangle^{(l)} W_p(\boldsymbol{\theta}_p) |\psi_{p-1}\rangle \right). \end{aligned} \quad (41)$$

Ignoring the unused ancillas we can therefore write the output of layer $l = p$ as

$$|\psi_p\rangle = \frac{1}{\Omega'_p} \left((1-\beta_p)|\psi_{p-1}\rangle + \beta_p W_p(\boldsymbol{\theta}_p)|\psi_{p-1}\rangle \right), \quad (42)$$

where $\Omega'_p = \sqrt{\pi_p}$ is a normalisation constant. Hence, assuming that the state $|\psi_{p-1}\rangle$ is correctly implemented by the procedure, we have shown that the output state $|\psi_p\rangle$ will be correctly implemented according to the quantum residual connection defined in Equation 22. As we have shown that $|\psi_1\rangle$ can be implemented correctly from the data input state $|\psi_0\rangle$, then by inductive reasoning $|\psi_l\rangle$ is correctly implemented for all $l \in [L]$.

The overall probability of success π_S will rely on all L qubits being successfully measured in the $|0\rangle^{(L)}$ state such that $\pi_S = \prod_{l=1}^L \pi_l$ and hence

$$\pi_S = \prod_{l=1}^L \left(1 - 2\beta_l(1-\beta_l)(1 - \text{Re}(\langle \psi_{l-1} | W_l(\boldsymbol{\theta}_l) | \psi_{l-1} \rangle)) \right). \quad (43)$$

as required. \square

We therefore show that the most general form of ResNet where connections can be skipped at every layer in a variational quantum circuit is probabilistically implementable. An example circuit architecture that demonstrates the process in the first two layers is shown in Figure 3. This implementation requires the number of ancilla qubits to equal L . For a more qubit efficient but less general version see Appendix E in which the number of ancilla used scales $\mathcal{O}(\log(L))$.

2.3 Probabilistic Scaling

During the proof in the previous section we found in Equation 40 that the probability π_l of measuring the l -th qubit in the $|0\rangle^{(L)}$ state, which is required for implementing the LCU method, to be

$$\pi_l = 1 - 2\beta_l(1-\beta_l)(1 - \text{Re}(\langle \psi_{l-1} | W_l(\boldsymbol{\theta}_l) | \psi_{l-1} \rangle)). \quad (44)$$

This is dependent on the strength of residual connection β_l , the quantum state of the previous step $|\psi_{l-1}\rangle$ and the variational circuit $W_l(\boldsymbol{\theta}_l)$.

Note that in general $\text{Re}(\langle \psi_{l-1} | W_l(\boldsymbol{\theta}_l) | \psi_{l-1} \rangle)$ lies in the range $[-1, 1]$. Therefore, the probability of success lies in the range $[1 - 4\beta_l(1 - \beta_l), 1]$. The worst-case scenario therefore occurs when $\beta_l = \frac{1}{2}$ as in this case the probability of success is within the range $[0, 1]$ and therefore there is a chance that the algorithm cannot be implemented. However, as β_l is varied to be closer to 0 or 1 this gives an increasing lower bound of $1 - 4\beta_l(1 - \beta_l)$ for the probability of success¹. This means that the probability of success lower bound can be

¹If $\beta_l = 1$ the probability of success equals 1, but would trivially mean that the skip connection is simply not performed. Likewise, if $\beta_l = 0$ then the success probability is equal to 1 but corresponds to not implementing the variational circuit $W_l(\boldsymbol{\theta}_l)$ at all.

adjusted to any desired value, as shown in Figure 4, by controlling the strength of the residual connection for the layer

$$|\psi_l\rangle = \frac{1}{\Omega'} \left((1 - \beta_l) |\psi_{l-1}\rangle + \beta_l W_l(\boldsymbol{\theta}_l) |\psi_{l-1}\rangle \right).$$

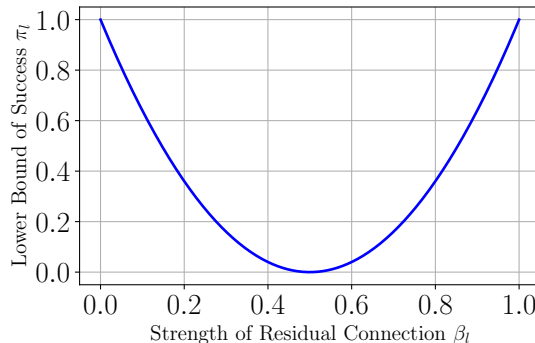


Fig. 4 Lower bound of success probability π_l for layer l in the LCU quantum native ResNet, as the strength of residual connection parameter β_l is adjusted. The lower bound is equal to $1 - 4\beta_l(1 - \beta_l)$.

The term $\text{Re}(\langle \psi_{l-1} | W_l(\boldsymbol{\theta}_l) | \psi_{l-1} \rangle)$ determines whether we will be close to the lower bound probability $1 - 4\beta_l(1 - \beta_l)$ or the upper bound of 1. We see that if $W_l(\boldsymbol{\theta}_l) = \mathbb{I}$ then we reach the upper bound and if $W_l(\boldsymbol{\theta}_l) = -\mathbb{I}$ we reach the lower bound. If restrictions were placed on the form $W_l(\boldsymbol{\theta}_l)$ can take there is potential to increase the lower bound probability even further.

As shown previously overall probability of success π_S will rely on all L qubits being successfully measured in the $|0\rangle$ state such that $\pi_S = \prod_{l=1}^L \pi_l$ and hence

$$\pi_S = \prod_{l=1}^L \left(1 - 2\beta_l(1-\beta_l)(1 - \text{Re}(\langle \psi_{l-1} | W_l(\boldsymbol{\theta}_l) | \psi_{l-1} \rangle)) \right). \quad (45)$$

Therefore, the lower bound of the overall probability of success is given by $\prod_{l=1}^L (1 - 4\beta_l(1 - \beta_l))$ which can be adjusted to be between 0 and 1 by varying the strength of the residual layers through the variables β_l .

If for a given architecture the probability of success for any layer is bounded between $[\pi_{\text{low}}, \pi_{\text{high}}]$. Then the probability of overall success must be bounded between $[\pi_{\text{low}}^L, \pi_{\text{high}}^L]$. In the case of $\pi_{\text{low}}, \pi_{\text{high}} < 1$, this means that the probability will decay exponentially with L , which is a key drawback of this method. However, if the number of layers used is chosen to scale logarithmically with the number of qubits $L =$

$\mathcal{O}(\log(n))$ then the algorithm can still run in time $\mathcal{O}(\text{poly}(n))$ in general, where n is the number of qubits for the target state register that initially contains $|\psi_0\rangle$. Furthermore, as discussed previously, the lower bounds can be adjusted by varying the strength of the residual connections for a given architecture.

2.4 Avoiding Barren Plateaus In Complex Models

We now provide a brief sketch of a possible avenue of avoiding barren plateaus in complex variational models. We shall consider a simple example of the two-layer case $L = 2$, where there is a residual connection between the input and the first layer, but no residual connection between the first and second layer. This can be implemented by setting $\beta_1 = \frac{1}{2}$ and $\beta_2 = 1$.

$$|\psi_1\rangle = \frac{1}{2}(|\psi_0\rangle + W_1(\boldsymbol{\theta}_1)|\psi_0\rangle), \quad (46)$$

$$|\psi_2\rangle = W_2(\boldsymbol{\theta}_2)|\psi_1\rangle. \quad (47)$$

hence

$$|\psi_2\rangle = \frac{1}{2}(W_2(\boldsymbol{\theta}_2)|\psi_0\rangle + W_2(\boldsymbol{\theta}_2)W_1(\boldsymbol{\theta}_1)|\psi_0\rangle). \quad (48)$$

This corresponds to applying the operator

$$A(\boldsymbol{\theta})_{\text{RES}} = \frac{1}{2}(W_2(\boldsymbol{\theta}_2) + W_2(\boldsymbol{\theta}_2)W_1(\boldsymbol{\theta}_1)). \quad (49)$$

We now consider some quantum encoded density matrix state ρ , where $\rho \equiv |\psi_0\rangle\langle\psi_0|$, which is evolved by this variational operator $A(\boldsymbol{\theta})_{\text{RES}}$ where the resulting loss function for the model with respect to an operator O is defined by

$$\langle O \rangle_{\rho, \boldsymbol{\theta}} = \text{Tr}(A(\boldsymbol{\theta})_{\text{RES}}\rho A(\boldsymbol{\theta})_{\text{RES}}^\dagger O), \quad (50)$$

hence

$$\begin{aligned} \langle O \rangle_{\rho, \boldsymbol{\theta}} &= \frac{1}{4} \left(\text{Tr}(W_2(\boldsymbol{\theta}_2)\rho W_2(\boldsymbol{\theta}_2)^\dagger O) \right. \\ &\quad + \text{Tr}(W_2(\boldsymbol{\theta}_2)W_1(\boldsymbol{\theta}_1)\rho W_1(\boldsymbol{\theta}_1)^\dagger W_2(\boldsymbol{\theta}_2)^\dagger O) \\ &\quad + \text{Tr}(W_2(\boldsymbol{\theta}_2)\rho W_1(\boldsymbol{\theta}_1)^\dagger W_2(\boldsymbol{\theta}_2)^\dagger O) \\ &\quad \left. + \text{Tr}(W_2(\boldsymbol{\theta}_2)W_1(\boldsymbol{\theta}_1)\rho W_2(\boldsymbol{\theta}_2)^\dagger O) \right). \quad (51) \end{aligned}$$

For simplicity of notation we shall assign a label to the derivative of each of the four terms.

$$X_1^{(\mu)} \equiv \frac{\partial}{\partial \theta_\mu} \text{Tr}(W_2(\boldsymbol{\theta}_2)\rho W_2(\boldsymbol{\theta}_2)^\dagger O) \quad (52)$$

$$X_2^{(\mu)} \equiv \frac{\partial}{\partial \theta_\mu} \text{Tr}(W_2(\boldsymbol{\theta}_2)W_1(\boldsymbol{\theta}_1)\rho W_1(\boldsymbol{\theta}_1)^\dagger W_2(\boldsymbol{\theta}_2)^\dagger O) \quad (53)$$

$$X_3^{(\mu)} \equiv \frac{\partial}{\partial \theta_\mu} \text{Tr}(W_2(\boldsymbol{\theta}_2)\rho W_1(\boldsymbol{\theta}_1)^\dagger W_2(\boldsymbol{\theta}_2)^\dagger O) \quad (54)$$

$$X_4^{(\mu)} \equiv \frac{\partial}{\partial \theta_\mu} \text{Tr}(W_2(\boldsymbol{\theta}_2)W_1(\boldsymbol{\theta}_1)\rho W_2(\boldsymbol{\theta}_2)^\dagger O). \quad (55)$$

where $\theta_\mu \in \boldsymbol{\theta}$ such that we can now write the gradient as

$$\frac{\partial \langle O \rangle_{\rho, \boldsymbol{\theta}}}{\partial \theta_\mu} = \frac{1}{4}(X_1^{(\mu)} + X_2^{(\mu)} + X_3^{(\mu)} + X_4^{(\mu)}). \quad (56)$$

A model is said to contain barren plateaus if $\forall \theta_\mu \in \boldsymbol{\theta}$ the following condition holds [43]

$$\text{Var}_{\boldsymbol{\theta}} \left(\frac{\partial \langle O \rangle_{\rho, \boldsymbol{\theta}}}{\partial \theta_\mu} \right) \leq F(n), \quad F(n) = \mathcal{O}\left(\frac{1}{b^n}\right), \quad b > 1. \quad (57)$$

where $\text{Var}_{\boldsymbol{\theta}}$ is the variance calculated over a uniform distribution of parameters $\boldsymbol{\theta}$. If we calculate this gradient variance term for the quantum ResNet example, we see that

$$\begin{aligned} \text{Var}_{\boldsymbol{\theta}} \left(\frac{\partial \langle O \rangle_{\rho, \boldsymbol{\theta}}}{\partial \theta_\mu} \right) &= \\ &\frac{1}{4} (\text{Var}_{\boldsymbol{\theta}}(X_1) + \text{Var}_{\boldsymbol{\theta}}(X_2) + \text{Var}_{\boldsymbol{\theta}}(X_3) + \text{Var}_{\boldsymbol{\theta}}(X_4) \\ &\quad + \text{Cov}_{\boldsymbol{\theta}}(X_1, X_2) + \text{Cov}_{\boldsymbol{\theta}}(X_1, X_3) + \text{Cov}_{\boldsymbol{\theta}}(X_1, X_4) \\ &\quad + \text{Cov}_{\boldsymbol{\theta}}(X_2, X_3) + \text{Cov}_{\boldsymbol{\theta}}(X_2, X_4) + \text{Cov}_{\boldsymbol{\theta}}(X_3, X_4)), \quad (58) \end{aligned}$$

where $\text{Cov}_{\boldsymbol{\theta}}$ is the covariance between two variables calculated over a uniform distribution of parameters $\boldsymbol{\theta}$ and we have dropped the superscripts of μ on the X terms for clarity of notation. There are many documented variational circuits that do not contain barren plateaus [35, 36, 44, 45]. Hence, selecting $W_2(\boldsymbol{\theta}_2)$, ρ , O to lie within any of these frameworks will lead to a situation in which the term $\text{Var}_{\boldsymbol{\theta}}(X_1)$ exhibits polynomial scaling $\text{Var}_{\boldsymbol{\theta}}(X_1) = \mathcal{O}\left(\frac{1}{\text{poly}(n)}\right)$. If this is the case, then it is possible that the gradient variance for the entire model could scale as $\text{Var}_{\boldsymbol{\theta}}\left(\frac{\partial \langle O \rangle_{\rho, \boldsymbol{\theta}}}{\partial \theta_\mu}\right) = \mathcal{O}\left(\frac{1}{\text{poly}(n)}\right)$, and hence barren plateaus will be avoided due to this beneficially scaling term under certain conditions: Firstly, the number of layers must scale as $L = \mathcal{O}(\log(n))$ in the general case, otherwise the beneficially scaling term may be exponentially suppressed. This requirement can be relaxed to $L = \mathcal{O}(\text{poly}(n))$ if considering special cases where less residual connections are used overall, as in the example above by setting some $\beta = 1$ or $\beta = 0$, or as demonstrated in the special case outlined in Appendix E. Secondly, it would also require that the covariance terms do not cancel out the beneficially scaling term.

The unique feature of this quantum ResNet implementation lies in its ability to sidestep barren plateaus while incorporating complex variational ansätze. Specifically, if the conditions for avoiding barren plateaus are met when considering only the $W_2(\theta_2)$ variational operator, then the $W_1(\theta_1)$ layer can be freely chosen to be any variational ansatz, even those known to exhibit barren plateaus, and the overall model could still avoid barren plateaus. This flexibility allows $W_1(\theta_1)$ to be chosen to be a circuit that is hard to simulate classically, ensuring that the overall model remains difficult to simulate. In other words, you may only need one layer that does not exhibit barren plateaus to avoid them completely, and you only need one layer that is hard to simulate classically to ensure the entire model is hard to simulate overall.

This approach provides a novel method for constructing VQC models that may avoid the trainability-classical simulability issue prevalent in the current literature; it has been reported that a wide class of VQCs that do not exhibit barren plateaus are classically simulatable [46], limiting the potential for quantum advantage. For example, it has been shown that for certain classes of VQC models, a likely requirement for trainability (the absence of barren plateaus) is that the dynamical Lie Algebra (DLA) dimension of the VQC is polynomial in size [47, 48]. Simultaneously, many VQC models with a polynomially sized DLA have also been shown to be classically simulatable [49], bringing into question their potential for quantum advantage. Beyond seeking quantum advantage for its own sake, it has also recently been demonstrated that polynomial sized DLA VQC models of this type are vulnerable to “weak privacy breaches” in which expectation value snapshots of quantum-encoded confidential data can be retrieved from the training gradients shared between nodes in a distributed learning setting; allowing potential attack agents to learn information about confidential input data [50]. This adds further urgency to find more complex quantum models that can still avoid the trainability issues associated with barren plateaus. However, by integrating a hard-to-simulate $W_1(\theta_1)$ (e.g., exponential size DLA) with a carefully designed trainable $W_2(\theta_2)$ (e.g., polynomial DLA), our model has the potential to remain non-classically simulatable while also remaining trainable. This potentially paves the way for the development of VQC models that leverage quantum complexity while maintaining efficient trainability. Furthermore, as the quantum ResNet construction allows for non-unitary operations that result in loss functions with parts deriving from both short and deep circuits simultaneously this means that many standard methods and

assumptions used for analysing VQC circuits may not apply, leaving ample opportunity for further research.

Note that the presence of non-unitary evolution terms, such as X_3 and X_4 , in the loss function gradient also introduces additional considerations regarding simulatability. As in general, these terms will not even be calculable on a quantum device using strictly unitary operations. The impact of these terms on simulatability is left as a subject for further research.

3 Average Pooling Layers

3.1 Quantum Average Pooling Implementation

In a Convolution Neural Network (CNN) it is common to find a pooling layer. This layer acts to reduce the dimension of the data by considering a tile of fixed size that passes over the data and performs some operation, such as averaging, on all the datapoints in the tile.

A classical average pooling layer consists of a pooling window of size $D \times D$ pixels that passes over an image consisting of $N \times N$ pixels, with a certain stride K_{STRIDE} [13–15]. We shall focus on the case where the pooling window moves across the image one pixel at a time, corresponding to a stride value $K_{\text{STRIDE}} = 1$. For each position of the pooling window, all pixels within the pooling window are averaged together, and this average is output as the value of a pixel in a new image. In classical techniques depending on the size of K_{STRIDE} and D the number of output pixels will be some number less than N^2 and hence the pooling corresponds to reducing the dimension of the image. In the quantum technique, there is no penalty for calculating all N^2 terms as the operations are done in parallel on the quantum state, hence we shall consider this case and leave the dimensionality reduction as a subroutine that can be implemented after the averaging.

We consider an image of $N \times N$ pixels where each pixel is indexed by i, j and the pixel colour value corresponds to $v_{i,j}$. If we focus on the average pooling window which is $D \times D$ in dimension, then classically we wish to redefine each pixel label by

$$v'_{i,j} = \frac{1}{D^2} \sum_{\Delta x=0}^{D-1} \sum_{\Delta y=0}^{D-1} T_{\Delta x, \Delta y}(v_{i,j}), \quad (59)$$

where $T_{\Delta x, \Delta y}$ is a pixel translation action which acts on the i, j indices of $v_{i,j}$ to retrieve the values other pixels through

$$T_{\Delta x, \Delta y}(v_{i,j}) = v_{i+\Delta x, j+\Delta y}, \quad (60)$$

so that they can be added to the average. The pixels accessed by $T_{\Delta x, \Delta y}$ define the pooling tile. For occasions in which the pooling window covers pixels outside the image, it is common to include some padding of the image [51], for example, any pixels outside the $N \times N$ region can be padded by zeros, giving a padded image of dimension $(N + 2D) \times (N + 2D)$.

There have been many investigations focused on finding quantum parallels to CNN models, whereby measurements are taken of certain qubits such that the dimensionality of the data is reduced. For example, in some setups the pooling layer corresponds to a variational ansatz followed by a measurement of a qubit [27]. In [25] an effective measurement was chosen corresponding to the symmetry and details of their specific problem concerning Quantum Phase Estimation. Although these popularised methods achieve the goal of pooling through reducing the dimensionality of the quantum state, they have not focused on giving a replication of an averaging pooling layer from classical CNN models for image data. In this section, we shall therefore demonstrate how LCU methods can be used to perform average pooling on quantum encoded image data. We shall utilise amplitude encoding with distinct coordinates x and y for the image, although any encoding for the data could be used, as long as the correct transformations are implemented with the LCU method.

Take an $N \times N$ image sample $(x_i, y_j, v_{i,j})$ where v represents the pixel colour value and x_i, y_j are the index coordinates of the pixel with $i, j \in [1, N]$. We shall utilise real amplitude encoding by defining a quantum state with two registers as

$$|\psi\rangle = \sum_{x_i, y_j} \frac{v_{i,j}}{\Omega} |x_i\rangle |y_j\rangle, \quad (61)$$

where $\Omega^2 = \sum v_{i,j}^2$ is a normalisation constant and $v_{i,j} \in \mathbb{R}$. Once we have an image encoded into a quantum state in this manner, we can consider the type of operation required by average pooling. In a simple case, we can consider only the x register for $D = 2$. We will need to apply an operation that takes $|x\rangle \rightarrow \frac{1}{\Omega'}(|x\rangle + |x \oplus 1\rangle)$ for some normalisation constant Ω' , to perform an averaging over pixels amplitudes. This will result in the state $|x\rangle$ having its amplitude transformed to the sum of the amplitudes of the $|x\rangle$ and $|x \oplus 1\rangle$ states before being normalised (and therefore averaged). This operation is implemented by $A_{\text{POOL}} = \frac{1}{2}(I + \text{SUBTRACT}_1)$, where $\text{SUBTRACT}_1|x\rangle = |x \oplus 1\rangle$ and $\text{ADD}_1|x\rangle = |x \oplus 1\rangle$. We can see that by taking

$$A_{\text{POOL}}^\dagger A_{\text{POOL}} = \frac{1}{4}(2\mathbb{I} + \text{ADD}_1 + \text{SUBTRACT}_1) \neq \mathbb{I}, \quad (62)$$

that it is not a unitary operation. Hence, to implement average pooling on a quantum device, we utilise LCU methods.

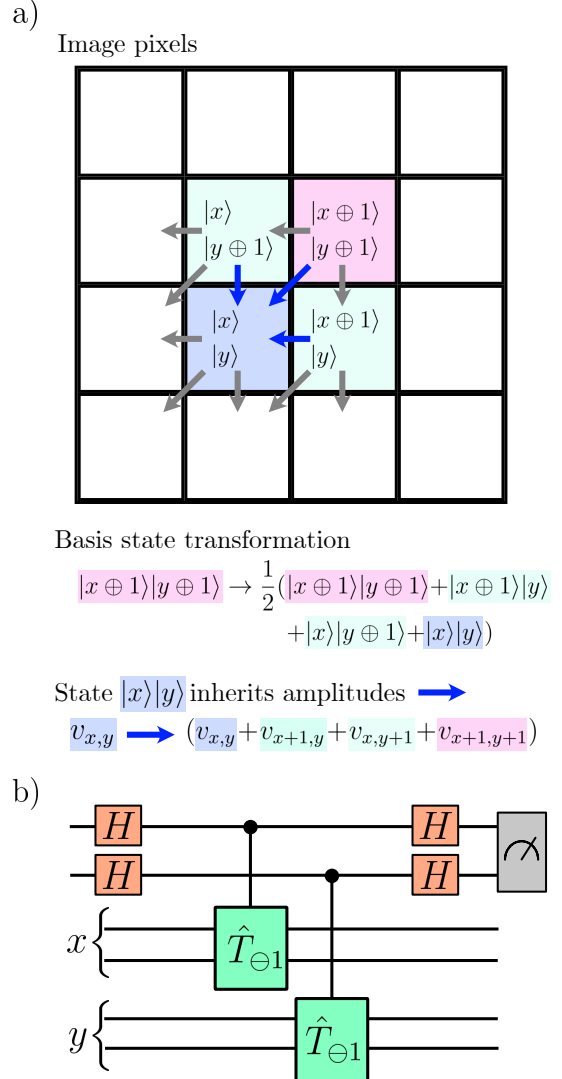


Fig. 5 a) Example of a 2×2 pooling window on a 4×4 pixel image indicating the desired transformation to perform average pooling. b) The circuit that implements the average pooling in this example through application of controlled $\hat{T}_{\ominus 1}$ operators to both registers.

Theorem 2 (Quantum Average Pooling) *It is possible to probabilistically implement an averaging pooling layer on an image that has been amplitude encoded into a quantum state as specified in Equation 61, such that*

the average pooling operation A_{POOL} has the effect

$$A_{POOL} \sum_{x_i, y_j} \frac{v_{i,j}}{\Omega} |x_i\rangle |y_j\rangle = \sum_{x_i, y_j} \frac{v'_{i,j}}{\Omega'} |x_i\rangle |y_j\rangle,$$

where

$$v'_{i,j} = \frac{1}{D^2} \sum_{\Delta x=0}^{D-1} \sum_{\Delta y=0}^{D-1} v_{i+\Delta x, j+\Delta y},$$

by using the LCU framework from Section 1.4. The terms Ω and Ω' are the normalisation constants for the initial and final states, respectively.

Proof For simplicity, we consider the ancilla qubits to be composed of two registers. We initialise these registers to the following

$$P_{\text{PREP}} |0\rangle^{\otimes k} |0\rangle^{\otimes k} = \frac{1}{D} \left(\sum_{\Delta x=0}^{D-1} |\Delta x\rangle \right) \left(\sum_{\Delta y=0}^{D-1} |\Delta y\rangle \right). \quad (63)$$

In this setting $|\Delta x\rangle$ and $|\Delta y\rangle$ correspond to the computational basis states of a Hilbert space of k qubits $\mathcal{H} = (\mathbb{C}^2)^{\otimes k}$, which are labelled by Δx and Δy . In this basis $|0\rangle \equiv |0\rangle^{\otimes k}$, $|1\rangle \equiv |0\rangle^{\otimes k-1} |1\rangle$ and $|2\rangle \equiv |0\rangle^{\otimes k-2} |1\rangle |0\rangle$ continuing for all values until $|2^k - 1\rangle \equiv |1\rangle^{\otimes k}$. The preparation operator therefore takes the form

$$P_{\text{PREP}} = \frac{1}{D} \left(\sum_{\Delta x=0}^{D-1} |\Delta x\rangle \right) \left(\sum_{\Delta y=0}^{D-1} |\Delta y\rangle \right) |0\rangle^{\otimes k} \langle 0|^{\otimes k} + \sum_{i=0}^{2^k-1} \sum_{j=1}^{2^k-1} (\dots) \langle i| \langle j| + \sum_{i=1}^{2^k-1} (\dots) \langle i| \langle 0|, \quad (64)$$

where (\dots) collects terms with $\langle i| \langle j|$ such that $i+j \geq 1$ and will therefore not be used in the algorithm and can be ignored. This can be clearly implemented by a unitary operation. It can also be shown that $T_{\Delta x, \Delta y}$ can be realised with a unitary operator. Binary addition is possible to implement on a quantum circuit [52] as shown in Figure 6 that shows $\text{ADD}_1|x\rangle = |x \oplus 1\rangle$. In general, we shall define a k adding operator as $\text{ADD}_k|x\rangle = |x \oplus k\rangle$, which can be formed by applying ADD_1 in series k times. The inverse of this operator, found by taking the Hermitian conjugate, will subsequently be the subtraction operator $\text{SUBTRACT}_k|x\rangle = |x \ominus k\rangle$.

In order for $T_{\Delta x, \Delta y}(v_{i,j})$ to recover the correct amplitude, we can utilise the ADD_k and SUBTRACT_k operators. We can therefore define $\hat{T}_{\Delta x, \Delta y}$ through the action of these operators as

$$\hat{T}_{\Delta x, \Delta y} |x_i\rangle |y_j\rangle = |x_i \ominus \Delta x\rangle |y_j \ominus \Delta y\rangle; \quad \Delta x, \Delta y > 0, \quad (65)$$

$$\hat{T}_{\Delta x, \Delta y} |x_i\rangle |y_j\rangle = |x_i \oplus |\Delta x|\rangle |y_j \oplus |\Delta y|\rangle; \quad \Delta x, \Delta y \leq 0. \quad (66)$$

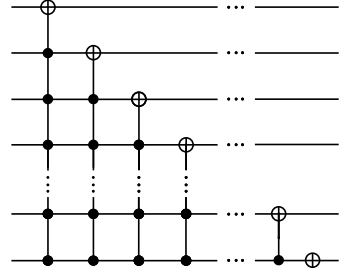


Fig. 6 Example circuit architecture to perform binary addition increasing all binary values by one. This takes $\text{ADD}_1|x\rangle = |x \oplus 1\rangle$ [52].

Now consider the action of $\hat{T}_{\Delta x, \Delta y}$ on the amplitude encoded image as

$$\begin{aligned} \hat{T}_{\Delta x, \Delta y} |\psi\rangle &= \hat{T}_{\Delta x, \Delta y} \left(\sum_{x_i, y_j} \frac{v_{i,j}}{\Omega} |x_i\rangle |y_j\rangle \right) \\ &= \sum_{x_i, y_j} \frac{v_{i,j}}{\Omega} |x_i \ominus \Delta x\rangle |y_j \ominus \Delta y\rangle \\ &= \sum_{x_i, y_j} \frac{v_{i,j}}{\Omega} |x_{i-\Delta x}\rangle |y_{j-\Delta y}\rangle. \end{aligned} \quad (67)$$

Relabelling the indices in the sum as $(i \rightarrow i + \Delta x)$ and $(j \rightarrow j + \Delta y)$ this can be written as

$$\hat{T}_{\Delta x, \Delta y} |\psi\rangle = \sum_{x_i, y_j} \frac{v_{i+\Delta x, j+\Delta y}}{\Omega} |x_i\rangle |y_j\rangle. \quad (68)$$

We can now define the selection operator as

$$\begin{aligned} S_{\text{SELECT}} |\Delta x\rangle |\Delta y\rangle |\psi\rangle &= |\Delta x\rangle |\Delta y\rangle \hat{T}_{\Delta x, \Delta y} |\psi\rangle \\ &= |\Delta x\rangle |\Delta y\rangle \sum_{x_i, y_j} \frac{v_{i+\Delta x, j+\Delta y}}{\Omega} |x_i\rangle |y_j\rangle, \end{aligned} \quad (69)$$

which corresponds to implementing controlled $\hat{T}_{\Delta x, \Delta y}$ operators, which are respectively applied when the ancilla is in the state $|\Delta x\rangle |\Delta y\rangle$. The selection operator is therefore unitary and can be applied on a quantum circuit.

Following the LCU procedure by first preparing the ancilla qubits gives

$$\begin{aligned} P_{\text{PREP}} |0\rangle^{\otimes k} |0\rangle^{\otimes k} |\psi\rangle &= \frac{1}{D} \left(\sum_{\Delta x=0}^{D-1} |\Delta x\rangle \right) \left(\sum_{\Delta y=0}^{D-1} |\Delta y\rangle \right) |\psi\rangle, \end{aligned} \quad (70)$$

applying the selection operator results in

$$\begin{aligned} S_{\text{SELECT}} P_{\text{PREP}} |0\rangle^{\otimes k} |0\rangle^{\otimes k} |\psi\rangle &= \frac{1}{D} \sum_{\Delta x=0}^{D-1} \sum_{\Delta y=0}^{D-1} |\Delta x\rangle |\Delta y\rangle \hat{T}_{\Delta x, \Delta y} |\psi\rangle. \end{aligned} \quad (71)$$

Applying the inverse preparation operator defined as

$$P_{\text{PREP}}^\dagger = \frac{1}{D} |0\rangle^{\otimes k} \langle 0|^{\otimes k} \left(\sum_{\Delta x=0}^{D-1} \langle \Delta x| \right) \left(\sum_{\Delta y=0}^{D-1} \langle \Delta y| \right)$$

$$+ \sum_{i=0}^{2^k-1} \sum_{j=1}^{2^k-1} |i\rangle|j\rangle(\dots) + \sum_{i=1}^{2^k-1} |i\rangle|0\rangle(\dots), \quad (72)$$

we can therefore see the state can be written as

$$\begin{aligned} & P_{\text{PREP}}^\dagger S_{\text{SELECT}} P_{\text{PREP}} |0\rangle^{\otimes k} |0\rangle^{\otimes k} |\psi\rangle \\ &= \frac{1}{D^2} |0\rangle^{\otimes k} |0\rangle^{\otimes k} \sum_{\Delta x=0}^{D-1} \sum_{\Delta y=0}^{D-1} \hat{T}_{\Delta x, \Delta y} |\psi\rangle \\ &+ \sum_{i=0}^{2^k-1} \sum_{j=1}^{2^k-1} |i\rangle|j\rangle(\dots) + \sum_{i=1}^{2^k-1} |i\rangle|0\rangle(\dots). \quad (73) \end{aligned}$$

We now wish to measure the ancilla qubits, discarding any states when $|0\rangle^{\otimes k} |0\rangle^{\otimes k}$ is not measured, hence we can ignore the (\dots) terms. The probability π_S of measuring the $|0\rangle^{\otimes k} |0\rangle^{\otimes k}$ state will therefore be

$$\pi_S = \left| \frac{1}{D^2} \sum_{\Delta x=0}^{D-1} \sum_{\Delta y=0}^{D-1} \hat{T}_{\Delta x, \Delta y} |\psi\rangle \right|^2. \quad (74)$$

After selecting only the cases where the ancillas are measured in the $|0\rangle^{\otimes k} |0\rangle^{\otimes k}$ state, the final state will be projected to

$$\begin{aligned} & \langle 0\rangle^{\otimes k} \langle 0\rangle^{\otimes k} P_{\text{PREP}}^\dagger S_{\text{SELECT}} P_{\text{PREP}} |0\rangle^{\otimes k} |0\rangle^{\otimes k} |\psi\rangle \\ &= \frac{1}{\sqrt{\pi_S} D^2} \sum_{\Delta x=0}^{D-1} \sum_{\Delta y=0}^{D-1} \hat{T}_{\Delta x, \Delta y} |\psi\rangle. \quad (75) \end{aligned}$$

where $\sqrt{\pi_S}$ term is required such that the state is normalised. Expanding out the operation of $\hat{T}_{\Delta x, \Delta y}$ it is possible to see that

$$\begin{aligned} & \frac{1}{\sqrt{\pi_S} D^2} \sum_{\Delta x=0}^{D-1} \sum_{\Delta y=0}^{D-1} \hat{T}_{\Delta x, \Delta y} |\psi\rangle \\ &= \frac{1}{\sqrt{\pi_S} D^2} \sum_{x_i, y_j} \sum_{\Delta x=0}^{D-1} \sum_{\Delta y=0}^{D-1} \frac{v_{i+\Delta x, j+\Delta y}}{\Omega} |x_i\rangle |y_j\rangle \\ &= \sum_{x_i, y_j} \frac{v'_{i,j}}{\Omega'} |x_i\rangle |y_j\rangle. \quad (76) \end{aligned}$$

The term $\Omega' = \sqrt{\pi_S} \Omega$ is the overall normalisation factor of the final state. Hence, the average pooling operation

$$v'_{i,j} = \frac{1}{D^2} \sum_{\Delta x=0}^{D-1} \sum_{\Delta y=0}^{D-1} v_{i+\Delta x, j+\Delta y}, \quad (77)$$

has been implemented on a quantum circuit. \square

In order to implement an average pooling layer with a pooling window size of $D \times D$ one needs to implement a linear combination D^2 unitaries via the LCU method, whereby the unitaries correspond to selecting the pixels within the tile. Due to the fact that we use two registers for x and y , this means that we

need $2D$ unitaries overall, which are controlled $\hat{T}_{\Delta x, 0}$ and $\hat{T}_{0, \Delta y}$ operators acting on the separate x and y target registers, which are controlled by the ancilla registers. A visualisation of the average pooling layer for a 2×2 pooling window is shown in Figure 5. In terms of the image boundaries, it would be possible to apply null padding to the image by introducing extra qubits in the $|0\rangle$ states. Without any padding, the quantum pooling window will treat the image as periodic and could include pixels from opposite sides of the image when located close to the image edge.

It is worth mentioning that classical CNNs perform this averaging as a means of dimensionality reduction, as the total number of averages taken is usually less than the total number of pixels in the image. In the quantum case, however, it takes no additional time to average every single pixel in the image, and therefore we presented this as the most general case. Subsequently, to truly perform the quantum analogue of pooling, certain values would be discarded to reduce the dimensionality of the problem. The exact method will depend on exactly what kind of dimensionality reduction is desired, although we discuss how this could be performed in Appendix D.

3.2 Algorithm Scaling

The advantage of average pooling layers is well documented in classical neural networks [53–55]. The method suggested in our work would allow this feature to be implemented on quantum encoded images in quantum machine learning models. The utility of this in the context of a quantum advantage will therefore be dependent on whether other quantum operations within the model can achieve some advantage over classical models. For example, recent empirical studies for amplitude encoded image data suggest that quantum models may in some circumstances display an improved robustness against adversarial attacks compared to classical methods [56, 57]. Indeed, theoretical guarantees on quantum robustness have recently been reported [58]. This is not the focus of our work, but the quantum pooling layers we introduce may be of use in further studies regarding quantum encoded image data. However, more concretely, we can show that assuming one has access to a quantum encoded image, that the quantum average pooling layer could be implemented faster than in the classical case. Specifically, the quantum parallelism allows all the pooling for every pixel to be calculated simultaneously, removing dependence on the total number of pixels in the operation.

Considering a stride value of 1, such that the pooling window moves one pixel at a time, to perform

the averaging classically, we need to average D^2 values for N^2 pixels, giving a scaling of at least $\Omega(N^2)$ with respect to N considering the amount of averaging operations required. If one has access to an amplitude encoded image, then to perform the averaging on this quantum state for all pixels requires D^2 operators in the linear combinations of unitaries, but these come from two different registers with D unitary operators each. This would therefore require ancilla qubits scaling as $k = \mathcal{O}(\log(D))$ in each ancilla register. The number of qubits required for the image encoding would be $\mathcal{O}(\log(N))$ in each target register for encoding both x and y . A key feature of this proposed method is that the N^2 scaling term associated with applying pooling classically is removed, as the nature of quantum superposition allows us to apply average pooling to every pixel in the image simultaneously. If we assume the image is provided as an amplitude encoded state and ignore for now the consideration of the probability of success inherent in the LCU method, this leads to a quadratic speedup over the classical case.

When considering the fact that this is a probabilistic algorithm with a chance of failure, the situation becomes slightly more complicated, as the probability will depend on the image itself. As shown previously, the probability of success is equal to

$$\pi_S = \left| \frac{1}{D^2} \sum_{\Delta x=1}^D \sum_{\Delta y=1}^D \hat{T}_{\Delta x, \Delta y} |\psi\rangle \right|^2.$$

If we had an image in which every pixel has the exact same colour value, we can effectively set $\hat{T}_{\Delta x, \Delta y} = \mathbb{I}$ and therefore $\pi_S = 1$. We expect real-world images to have pixels that are close in colour value to other local pixels nearby on average with the exceptions occurring at the edges of subjects within the image. We therefore expect the probability to remain relatively stable overall, although one could construct adversarial example images that result in low probabilities. To gain a practical understanding of this probability scaling we considered the MNIST fashion dataset [16], we empirically show the scaling of the probability of success with respect to D and N in Figure 7 and Figure 8, respectively. These results indicate that the probability of success decreases but levels off after a certain point as D increases, and that there is no discernible trend when increasing N . These results align with our intuition for real-world images. The general structure and content of real-world images (and their local pixel similarities) remain consistent as N increases; therefore, there should be no discernible decrease in π_S from increasing N . On the other hand, increasing D means considering a larger neighbourhood of pixels. Initially,

as D increases, the probability of encountering edges within this neighbourhood also increases, causing π_S to decrease. However, beyond a certain point, further increasing D adds less new information because most of the image regions are already accounted for and edges covered, so π_S levels off. The exact probability will be very image dependent; there may also exist techniques to prepare images such that the probabilities are improved, which we leave as an open question for further research.

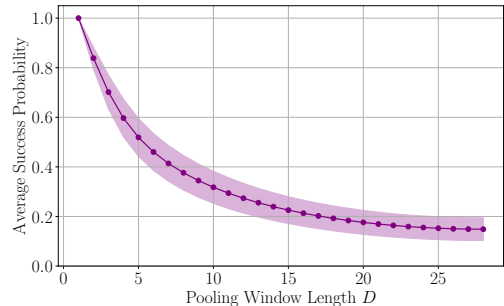


Fig. 7 Average success probability of the LCU procedure for implementing an average pooling layer as the pooling window dimension D is increased, while the image size is set to $N = 28$. The average is taken over 100 image samples from the MNIST database [16], with the shaded area indicating the standard deviation of the samples.

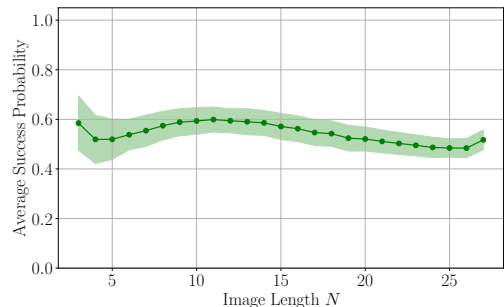


Fig. 8 Average success probability of the LCU procedure for implementing an average pooling layer as the image size N is increased, while the pooling window size is kept constant at $D = 3$. The average is taken over 100 image samples from the MNIST database [16], with the shaded area indicating the standard deviation of the samples.

4 Irreducible Subspace Projections

In order to discuss the irreducible subspace projections circuit, we first give a brief overview of representation theory definitions.

4.1 Representation Theory Preliminaries

Following standard texts on group and representation theory [59, 60] we provide a brief summary and introduction to the underlying mathematical framework utilised in this section.

The definition of a representation of a group G can be given as

Definition 1 (Representation) *A representation of a group G refers to a pair (U, V) , where V is a vector space and U is a group homomorphism $U : G \rightarrow GL(V)$, where $GL(V)$ is the general linear group of invertible matrices that acts on the vector space V of the representation. The homomorphism maps group elements $g \in G$ to matrices $U_g \in GL(V)$.*

Often either the homomorphism U , the vector space V or the image subgroup $U_G \subseteq GL(V)$ can be referred to as the “representation” depending on context.

Definition 2 (Subrepresentation) *For a given representation (U, V) a subrepresentation is a vector subspace $W \subseteq V$ for which any vector $w \in W$ remains within W when acted on by any representation of the group, that is, $U_g w \in W, \forall g \in G$.*

Definition 3 (Irreducible Representation) *If a representation does not contain any non-trivial subrepresentations (the trivial spaces being the empty subspace $\{0\}$ and the entire space V) then it is said to be an irreducible representation.*

If a representation does contains a non-trivial subrepresentation, then it is called a reducible representation. Representations can often be decomposed into a direct sum of their irreducible representations, in which case they are called completely reducible. Maschke’s Theorem [61] states that any finite-dimensional representation of a finite group G over a field F will be completely reducible (so long as the field characteristic does not divide the order of the group). It is also the case that every finite-dimensional

representation of compact Lie groups is completely reducible [62]. If a representation (U, V) is completely reducible, then there exists a basis in which we can write U_g as

$$U_g \rightarrow \bigoplus_{r=1}^R \bigoplus_{j=1}^{m_r} u_g^{(r)} = \bigoplus_{r=1}^R u_g^{(r)} \otimes \mathbf{I}_{m_r}, \quad (78)$$

where $(u^{(r)}, V_r)$ are the irreducible representations indexed by $r \in [1, R]$, where R is the total number of irreducible representations. In this work we will often refer to r as the irreducible representation for simplicity, although strictly it is the label that indexes the irreducible representations $(u^{(r)}, V_r)$. The quantity m_r is called the multiplicity of the irreducible representation. We can also define the degree of a representation as $n_r \equiv \dim(V_r)$. In this basis U_g is in a block-diagonal form. This change of basis also decomposes the representation vector space V as

$$V \rightarrow \bigoplus_{r=1}^R V_r \otimes \mathbb{C}^{m_r}. \quad (79)$$

The conjugacy class of a group and the character of a representation for a given group element can be defined as

Definition 4 (Conjugacy Class) *For a group G two given elements $g, h \in G$ are said to be conjugate if $\exists x \in G$ such that*

$$g = xhx^{-1},$$

and hence the conjugacy class can be defined as

$$C_{(g)} = \{xgx^{-1} \mid x \in G\},$$

corresponding to the set of all elements that are conjugate to g .

Definition 5 (Character) *For a representation (U, V) of the group G , the character can be defined as*

$$\chi_U(g) = \text{Tr}(U_g),$$

which is the trace of the representation of g on V . For the irreducible representations $(u^{(r)}, V_r)$ indexed by r we shall define $\chi_{u^{(r)}}(g) \equiv \chi_r(g)$ for simplicity.

In particular, as the trace permits cyclic permutation, this means that $\chi_r(xgx^{-1}) = \chi_r(g)$ and therefore $\chi_r(g)$ is constant on the conjugacy classes of G . i.e., if $g_1, g_2 \in C_{(g_1)}$ then $\chi_r(g_1) = \chi_r(g_2)$. It is also worth noting that as the identity element corresponds to an identity matrix, taking the trace of an identity matrix will result in the fact that $\chi_r(I) = \dim(V_r)$. Hence, the

degree of an irreducible representation can be found by $n_r = \dim(V_r) = \chi_r(I)$.

We will now introduce a key result of this work regarding projecting quantum encoded states to any linear combination of irreducible subspaces of a given finite group.

4.2 Subspace Projection Circuit

We start by observing a result from the representation theory of finite groups which states [63]

Theorem 3 (Irreducible Subspace Projection) *Let $U : G \rightarrow GL(V)$ be a representation of G . The canonical decomposition into an irreducible representation is given by $V = V_1 \oplus V_2 \oplus \dots \oplus V_R$, where the irreducible representations have characters χ_1, \dots, χ_R and degrees n_1, \dots, n_R . Then the projection \hat{P}_r of V onto the space V_r is given by:*

$$\hat{P}_r = \frac{n_r}{|G|} \sum_{g_i \in G} \chi_r(g_i)^* U_{g_i}, \quad (80)$$

where $\chi_r(g_i)$ is the character of group element $g_i \in G$ for irreducible representation r , and U_{g_i} is the matrix representation of group element $g_i \in G$ acting on the space V .

This is a known result in representation theory; for more details, see reference texts such as [59, 63]. In this section, we explore a method for implementing this projection on a quantum circuit using the Linear Combination of Unitaries (LCU) technique. Specifically, we demonstrate the practicality of realising the projection described in Theorem 3 on a quantum device. In the most comprehensive scenario, we establish that a quantum circuit can execute combinations of such \hat{P}_r projections at the same time via the LCU method.

Theorem 4 (Quantum Generic Irreducible Subspace Projection) *Let $|\psi\rangle \in V = (\mathbb{C}^2)^{\otimes n}$ be a quantum state encoded on n qubits. Let $U : G \rightarrow SU(2^n)$ be a unitary representation of a compact finite group G , where the representatives for group elements $g_i \in G$ are denoted $U_{g_i} \in SU(2^n)$ and are unitary operators that acts on $|\psi\rangle$ and can be implemented in a quantum device. Utilising the Linear Combination of Unitaries framework on a quantum circuit, one can probabilistically apply a linear combination of irreducible representation projections*

$$\sum_{r=1}^R a_r \hat{P}_r |\psi\rangle = \frac{1}{\Omega'} \sum_{r=1}^R a_r \left(\frac{n_r}{|G|} \sum_{g_i \in G} \chi_r(g_i)^* U_{g_i} |\psi\rangle \right), \quad (81)$$

such that \hat{P}_r projects $|\psi\rangle \in V$ to the subspace V_r corresponding to the irreducible representation subspace indexed by r with degree n_r . The constants a_r can be freely chosen, Ω' is the normalisation constant for the final state after projection, and R is the total number of irreducible representations.

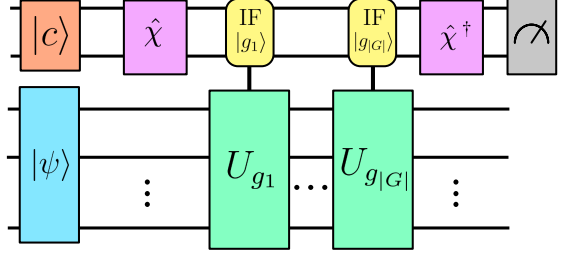


Fig. 9 The general irreducible representation projection circuit. The upper register consisting of k qubits is prepared into a superposition state $|c\rangle$, where the basis states $|b_r\rangle$ are labelled by the irreducible representations r . The operator $\hat{\chi}$ then takes each irreducible representation labelled basis state to its corresponding group element labelled basis state multiplied by the correct character. Each group element labelled basis state $|g_i\rangle \equiv |b_i\rangle$ where $g_i \in G$ then controls the application of its corresponding representation on the quantum states in the lower register, represented by $U_{g_i} \in SU(2^n)$. This is achieved by using multi-qubit control gates, such that if the ancilla is in the state $|g_i\rangle$, the operator U_{g_i} is applied and nothing else. This is demonstrated in the graphic using yellow boxes for these conditional control gates, which are controlled by specific multi-qubit basis states $|g_i\rangle$. These can be constructed as multi-qubit control gates along with the correct implementation of X gates to ensure the controlled action U_{g_i} is only applied when the ancilla register is in the correct basis state $|g_i\rangle$. We apply $\hat{\chi}^\dagger$ on the upper register and then measure and post-select for the $|b_1\rangle \equiv |0\rangle^{\otimes k}$ state. We demonstrate this will create the appropriate combinations of projections onto the desired subspaces with the proportion of each projector determined by the initialisation of the state $|c\rangle$.

Proof As we intend to implement a linear combination of projections, we shall consider a slightly more general form of the LCU method. We first perform a pre-initialisation step on the k ancilla qubits, initially in the basis state $|b_1\rangle$, using an operator $\hat{\gamma}$ to prepare the state $|c\rangle = \hat{\gamma}|b_1\rangle$ defined as

$$|c\rangle = \frac{1}{\Omega} \sum_{r=1}^R a_r n_r |b_r\rangle, \quad (82)$$

where a_r can be chosen to adjust the relative amounts of a given representation, n_r is the degree of the representation, and $\Omega = \sum_{r=1}^R |a_r n_r|^2$ is a normalisation constant for the quantum state. The states

$\{|b_j\rangle\}_{j \in [1, 2^k]} \in (\mathbb{C}^2)^{\otimes k}$ are basis states of the 2^k dimensional Hilbert space for the k qubit ancilla register denoted by $\mathcal{H} = (\mathbb{C}^2)^{\otimes k}$. They can be taken to be computational basis states. We highlight that after this pre-initialisation the ancilla register is in a combination up to R basis states, which are indexed by the irreducible representations r . The inclusion of the n_r term here ensures that the representation weightings are correct later on. At this point, every state $|b_r\rangle$ corresponds to a different irreducible representation of the group G . We define $r = 1$ to correspond to the trivial representation.

The next step corresponds to applying an operator that takes each representation labelled state $|b_r\rangle$ into a sum of basis states $|b_i\rangle$, $i \in [1, |G|]$ which are now labelled by the elements of the group $g_i \in G$, where each basis state $|b_i\rangle$ inherits a weighting according to the character $\chi_r(g_i)^*$ corresponding to the representation r and the relevant group element g_i . To help improve readability, we define $|g_i\rangle \equiv |b_i\rangle$. These correspond to the same basis states in the ancilla register, but emphasises the fact that are labelled by the group elements g_i .

As we consider a combination of multiple projections at the same time, then, in order to maintain generality of our framework, instead of requiring $P_{\text{PREP}, r}$ to be a different operator for each individual irreducible representation (indexed by r) as would be the standard case in LCU methods, we will consider a generalised preparation operator corresponding to the unitary $\hat{\chi}$ which has the effect of applying the correct character for every irreducible representation r and every group element $g_i \in G$ such that

$$\hat{\chi}|b_r\rangle = \frac{1}{\sqrt{|G|}} \sum_{g_i \in G} \chi_r(g_i)^* |g_i\rangle. \quad (83)$$

where in the most general form

$$\hat{\chi} = \frac{1}{\sqrt{|G|}} \sum_{r=1}^R \sum_{g_i \in G} \chi_r(g_i)^* |g_i\rangle \langle b_r| + \sum_{r=R+1}^{2^k} (\dots) \langle b_r|, \quad (84)$$

where the terms grouped together as $\sum_{r=R+1}^{2^k} (\dots) \langle b_r|$ will not be used in the algorithm and can hence be ignored. Implementing this corresponds to constructing a matrix that contains the character of every group element for every irreducible representation. This matrix will have the form

$$[\hat{\chi}]_{i,j} = \begin{cases} \frac{1}{\sqrt{|G|}} \chi_j(g_i), & \text{if } i \in [1, |G|], j \in [1, R] \\ 0 & \text{if } i \in (|G|, 2^k], j \in [1, R] \\ \frac{1}{\sqrt{|G|}} u_{i,j} & \text{if } i \in [1, 2^k], j \in (R, 2^k], \end{cases} \quad (85)$$

where the $u_{i,j}$ will never affect the algorithm, but are required as the matrices involved must be of size 2^k .

The first R columns correspond to the vectors that contain the characters for each element in a given representation. Considering the character orthogonality theorem [64] which states that

$$\frac{1}{|G|} \sum_{g_i \in G} \chi_j(g_i) \chi_k(g_i)^* = \delta_{j,k}, \quad (86)$$

this means that the character vectors of irreducible representations form an orthonormal basis. The $u_{i,r}$ terms can be chosen utilising the Gram-Schmidt procedure or otherwise to ensure that all column vectors of $\hat{\chi}$ form an orthonormal basis. A matrix whose column vectors form an orthonormal basis is unitary. Hence, our generalised preparation step $P_{\text{PREP}} = \hat{\chi}$ can be implemented on a quantum circuit.

The S_{SELECT} operator can be implemented by applying the unitary quantum gate representation $U_g \in SU(2^n)$ to the n qubit target state $|\psi\rangle \in V = (\mathbb{C}^2)^{\otimes n}$ for each corresponding group element $|g_i\rangle$ in the ancilla register

$$S_{\text{SELECT}}|g_i\rangle|\psi\rangle = |g_i\rangle U_{g_i}|\psi\rangle. \quad (87)$$

As long as G is a compact group, there will be unitary irreducible representations U_{g_i} via the Peter-Weyl theorem [65]. Hence U_{g_i} can be implemented in a quantum circuit for compact groups G . Using controlled gates U_{g_i} , in which the operation U_{g_i} is applied only when the ancilla qubit is in the state $|g_i\rangle$, then the operator S_{SELECT} is successfully implemented.

We have shown that the preparation and selection operators can be implemented on a quantum circuit, now all that remains is to combine the operators together to view the full action of the LCU procedure. Pre-initialising the ancillas

$$\hat{\gamma}|b_1\rangle|\psi\rangle = \frac{1}{\Omega} \sum_{r=1}^R a_r n_r |b_r\rangle|\psi\rangle, \quad (88)$$

followed by applying preparation operator $\hat{\chi}$ on the ancillas gives

$$\hat{\chi} \hat{\gamma}|b_1\rangle|\psi\rangle = \frac{1}{\Omega} \sum_{r=1}^R a_r n_r \frac{1}{\sqrt{|G|}} \sum_{g_i \in G} \chi_r(g_i)^* |g_i\rangle|\psi\rangle. \quad (89)$$

The selection operator applied to the circuit can then be written

$$\begin{aligned} S_{\text{SELECT}} \hat{\chi} \hat{\gamma}|b_1\rangle|\psi\rangle \\ = \frac{1}{\Omega} \sum_{r=1}^R a_r n_r \frac{1}{\sqrt{|G|}} \sum_{g_i \in G} \chi_r(g_i)^* |g_i\rangle U_{g_i}|\psi\rangle. \end{aligned} \quad (90)$$

The conjugate $\hat{\chi}$ term can be written as

$$\hat{\chi}^\dagger = \frac{1}{\sqrt{|G|}} \sum_{r=1}^R \sum_{g_i \in G} \chi_r(g_i) |b_r\rangle \langle g_i| + \sum_{r=R+1}^{2^k} |b_r\rangle (\dots), \quad (91)$$

where $\sum_{r=R+1}^{2^k} |b_r\rangle(\dots)$ represents terms that will not end up contributing and hence we can ignore. Applying the conjugate $\hat{\chi}^\dagger$ term, and separating out terms that will not be used further we find

$$\hat{\chi}^\dagger S_{\text{SELECT}} \hat{\chi} |b_1\rangle |\psi\rangle = \frac{1}{\Omega} \sum_{r=1}^R a_r \frac{n_r}{|G|} \sum_{g_i \in G} |b_1\rangle \chi_1(g_i) \chi_r(g_i)^* U_{g_i} |\psi\rangle + \sum_{r=2}^{2^k} |b_r\rangle(\dots), \quad (92)$$

where we can ignore all terms $\sum_{r=R+1}^{2^k} |b_r\rangle(\dots)$ as they will be discarded if ever measured. Note that since $r=1$ is defined as the trivial representation, it follows that $\chi_1(g_i) = 1, \forall g_i \in G$. We now measure the ancilla qubits and find that they will be found in the state $|b_1\rangle$ with a probability π_S given by

$$\pi_S = \left| \frac{1}{\Omega} \sum_{r=1}^R a_r \frac{n_r}{|G|} \sum_{g_i \in G} \chi_r(g_i)^* U_{g_i} |\psi\rangle \right|^2. \quad (93)$$

By only retaining states in which the ancilla was measured in the $|b_1\rangle$ state, we will have prepared the state

$$\begin{aligned} & \langle b_1 | \hat{\chi}^\dagger S_{\text{SELECT}} \hat{\chi} |b_1\rangle |\psi\rangle \\ &= \frac{1}{\Omega'} \sum_{r=1}^R a_r \frac{n_r}{|G|} \sum_{g_i \in G} \chi_r(g_i)^* U_{g_i} |\psi\rangle, \end{aligned} \quad (94)$$

where $\Omega' = \sqrt{\pi_S} \Omega$ is the normalisation constant of the final state, as required. \square

A simple corollary regarding the special case in which during the pre-initialisation stage $a_{r'=r} = 1$ and $a_{r' \neq r} = 0$, such that only one irreducible representation is selected.

Corollary 4.1 (Quantum Individual Subspace Projection) *The projection given in Theorem 3 can be probabilistically implemented on an n qubit quantum state $|\psi\rangle \in V = (\mathbb{C}^2)^{\otimes n}$ by utilising a Linear Combination of Unitaries in a quantum circuit where*

$$\hat{P}_r |\psi\rangle = \frac{n_r}{\Omega' |G|} \sum_{g_i \in G} \chi_r(g_i)^* U_{g_i} |\psi\rangle, \quad (95)$$

such that \hat{P}_r projects $|\psi\rangle$ from the space V to an irreducible representation subspace V_r .

This shows that the LCU method can be adapted through careful selection of the preparation and selection operators to reproduce the projection onto any combination of irreducible representations. An overall schematic of the representation projection circuit is shown in Figure 9. Note that after the projection, the state may no longer be a pure state.

4.2.1 Circuit Scaling

In order for k ancilla qubits to have a basis state for each group element representation of G it would require $2^k \geq |G|$. Hence, the number of qubits required scales as $k \approx \mathcal{O}(\log(|G|))$. However, the character implementation unitary $\hat{\chi}$ which is used in the ancilla preparation stage has a dimension that scales with $\mathcal{O}(|G|)$ which may be prohibitive in certain cases. For example, if G is taken to be the permutation group $G = S_n$, where the representation operators $U_{\sigma_i}, \sigma_i \in S_n$ correspond to permuting n qubits in the target state, then we require $k \approx \mathcal{O}(\log(n!)) \approx \mathcal{O}(n \log(n))$ ancilla qubits, however we are required to initialise a unitary of size $\mathcal{O}(n!)$, which may be difficult. A proposed solution outlined in Appendix A is to utilise a smaller version of $\hat{\chi}$ corresponding to the character table where each ancilla qubit state represents a conjugacy class rather than individual group elements. In this case, the size of the unitary required could be significantly reduced, as it would scale only with the number of conjugacy classes, denoted by $|\mathcal{C}|$. Hence, this alternative implementation would require ancilla qubits of order $\mathcal{O}(\log(|\mathcal{C}|))$ to encode the character table state, but then it would also require $|\mathcal{C}|$ extra registers, one per conjugacy class, with sufficient qubits to produce a superposition of states for every element in the conjugacy class. This means more qubits are required in total, but the unitary is easier to implement. The number of conjugacy classes in S_n , for example, that is approximately approached in the asymptotic limit is

$$|\mathcal{C}_n| \approx \frac{1}{4n\sqrt{3}} \exp\left(\pi\sqrt{\frac{2n}{3}}\right); n \rightarrow \infty, \quad (96)$$

which is super-polynomial but sub-exponential [59]. This would be a significant improvement in scaling compared to $\mathcal{O}(n!)$. This allows a trade-off between total qubits and the ease of unitary preparation. Note that in this section, we introduced a very general framework, and improvements in circuit efficiency to implement $\hat{\chi}$ may well be possible for specific groups, representations, and data types.

4.2.2 Probabilistic Scaling

The probability of success π_S is shown in Equation 93 which is equal to the probability of measuring the ancillas in the $|b_1\rangle$ state. This can be simplified by utilising the result of Theorem 4 to observe that

$$\pi_S = \left| \frac{1}{\Omega} \sum_{r=1}^R a_r \hat{P}_r |\psi\rangle \right|^2. \quad (97)$$

Any quantum state can be written as a decomposition in terms of its components on the irreducible subspaces

$$|\psi\rangle = \bigoplus_{r=1}^R \bigoplus_{j=1}^{m_r} |\psi_r\rangle_j, \quad (98)$$

where m_r is the multiplicity of representation r . We define $|\psi_r\rangle \equiv \bigoplus_{j=1}^{m_r} |\psi_r\rangle_j$ and see that it denotes the component of $|\psi\rangle$ that occupies the subspaces of the irreducible representation r . After $|\psi\rangle$ is projected by \hat{P}_r onto the irreducible subspace of r it will equal $|\psi_r\rangle$. Noting that $|\psi_r\rangle$ will be orthogonal for different r values, we can therefore write

$$\pi_S = \frac{1}{\Omega^2} \sum_{r=1}^R |a_r|^2 \langle \psi_r | \psi_r \rangle. \quad (99)$$

Therefore, the probability of success depends on the amount that the initial state $|\psi\rangle$ occupies the relevant irreducible subspaces in the projection. The normalisation condition in the general state means that $\langle \psi | \psi \rangle = \sum_r \langle \psi_r | \psi_r \rangle = 1$. In the case that we project fully to one specific space $a_r = 1, a_{r' \neq r} = 0$ then

$$\pi_S = \langle \psi_r | \psi_r \rangle, \quad (100)$$

which will depend on how much of the state $|\psi\rangle$ lies in the subspace of irreducible representation r . If $|\psi\rangle$ lies fully within the space, then $\pi_S = \langle \psi_r | \psi_r \rangle = 1$. Conversely, if $|\psi\rangle$ has no components in the subspace for irreducible representation r then $\pi_S = \langle \psi_r | \psi_r \rangle = 0$ and the algorithm is impossible to run. An advantage of the additional control introduced by the a_r parameters is that we can freely choose the weightings to potentially improve the probability of success. In general, the probability of success will depend greatly on data encoding and choice of representations.

4.3 Symmetry Invariant Encodings for Point Cloud Data

The previous subsection outlines how a quantum state can be projected to any irreducible representation of a finite group, or linear combination thereof. In this subsection, we highlight how certain irreducible representation subspaces may be useful for a specific type of data when encoded into a quantum state, namely point cloud data.

A point cloud is a collection of three-dimensional vectors (the points) that when viewed as a collective represent an image. Amongst other applications they are often associated with computer vision algorithms, as a primary method for performing three-dimensional imaging is the use of the Light Detection and Ranging

(LiDAR) system, which produces point clouds as its data output [66]. We can consider a point cloud P as a set of three-dimensional vectors $P = \{\mathbf{p}_1, \mathbf{p}_2, \dots, \mathbf{p}_n\}$ that overall forms an image. We can consider a form of quantum encoding in which each individual point \mathbf{p}_i is encoded into a quantum state $|\mathbf{p}_i\rangle$ leading to a separable quantum state for the overall point cloud as

$$|P\rangle = |\mathbf{p}_1\rangle \otimes |\mathbf{p}_2\rangle \otimes \dots \otimes |\mathbf{p}_n\rangle. \quad (101)$$

The states $|\mathbf{p}_i\rangle$ could be single qubits, in which case the total number of qubits in this target register would be n . However, in general, each $|\mathbf{p}_i\rangle$ could be a state encoded on t qubits, in which case we can consider each $|\mathbf{p}_i\rangle$ as a 2^t -dimensional qudit and n would denote the number of qudits in the system that encodes $|P\rangle$.

4.3.1 Permutation Invariance

The ordering of the points within the set P does not affect the overall image; however, in general a machine learning algorithm may output different results depending on the ordering of the points in the data input array. A solution to prevent this by utilising permutation symmetric encodings for point clouds was suggested in previous work [18] where a quantum superposition of all possible permutations was used, leading to a permutation invariant quantum encoding such that

$$|P\rangle_{\text{perm}} = \frac{1}{\Omega'} \sum_{\sigma \in S_n} |\mathbf{p}_{\sigma^{-1}(1)}\rangle \otimes |\mathbf{p}_{\sigma^{-1}(2)}\rangle \otimes \dots \otimes |\mathbf{p}_{\sigma^{-1}(n)}\rangle. \quad (102)$$

This previous work can be viewed as a special case of the LCU method described previously, in which the group is S_n and the state $|P\rangle$ is projected to the symmetric irreducible representation subspace (in which the character for all group elements is equal to one). The representations of the group elements $\sigma \in S_n$ that act on $|P\rangle$ are denoted by U_σ and correspond to SWAP gates that permute the constituent states $|\mathbf{p}_i\rangle$ accordingly. This projection would correspond to applying the projector

$$\sum_{\sigma \in S_n} U_\sigma |P\rangle = \frac{1}{\Omega'} \sum_{\sigma \in S_n} |\mathbf{p}_{\sigma^{-1}(1)}\rangle \otimes \dots \otimes |\mathbf{p}_{\sigma^{-1}(n)}\rangle, \quad (103)$$

providing the result proposed in Equation 102 and recreating the work of [18] as a special case of a more general framework.

4.3.2 Rotational Invariance

The novelty of the projection technique we propose in the LCU framework is that it allows expansion to

many other possible symmetries beyond permutation invariance. Here we shall outline another example, rotationally invariant encodings of point clouds that contain four points utilising an $SU(2)^{\otimes 4}$ invariant encoding. This is motivated by the fact that $SU(2)$ is the double cover of $SO(3)$, which is the group that corresponds to rotations in three dimensions, which means that each element of $SO(3)$ corresponds to exactly two elements in $SU(2)$.

In this framework, we consider point clouds in which the points \mathbf{p}_i are represented in spherical coordinates $\mathbf{p}_i = (r_i, \theta_i, \phi_i)$. We shall ignore the radial component r_i for the sake of simplicity, although this could be included in any practical implementation in an appropriate manner.

We propose an encoding in which for each point $\mathbf{p}_i = (r_i, \theta_i, \phi_i)$ is encoded into the following quantum state

$$|\mathbf{p}_i\rangle = \cos\left(\frac{\theta_i}{2}\right)|0\rangle + e^{i\phi_i}\sin\left(\frac{\theta_i}{2}\right)|1\rangle, \quad (104)$$

such that the θ_i and ϕ_i angle of the point is encoded into the respective angles of a single qubit in the Bloch sphere representation.

Rotation of a point cloud corresponds to rotating every individual point by the same amount and in the same direction such that $(r_i, \theta_i, \phi_i) \rightarrow (r_i, \theta_i + \delta\theta, \phi_i + \delta\phi) \forall i \in [1, n]$. Considering this in terms of the quantum encoded state above, it would correspond to the application of the same rotation $U_{SU(2)} \in SU(2)$ on each qubit $|\mathbf{p}_i\rangle$, rotating every qubit state about the Bloch sphere by the same amount. In order to have a quantum encoded point cloud that is invariant to rotations of the point cloud, it would require the following invariance

$$\begin{aligned} & |\mathbf{p}_1\rangle|\mathbf{p}_2\rangle|\mathbf{p}_3\rangle|\mathbf{p}_4\rangle \\ &= U_{SU(2)}|\mathbf{p}_1\rangle U_{SU(2)}|\mathbf{p}_2\rangle U_{SU(2)}|\mathbf{p}_3\rangle U_{SU(2)}|\mathbf{p}_4\rangle, \end{aligned} \quad (105)$$

which would be invariance under the action $SU(2)^{\otimes 4}$.

We consider irreducible representations of the group S_4 , where the representations of group elements $\sigma \in S_4$ correspond to the SWAP gates $U_\sigma = \text{SWAP}_\sigma$ that permute the constituent points $|\mathbf{p}_i\rangle$ accordingly. We are able to use this because Schur-Weyl duality (see Appendix B for a detailed discussion) provides a relation between irreducible finite-dimensional representations between the symmetric group and general linear group. This means that for the one-dimensional trivial representation of $SU(2)^{\otimes n}$ of multiplicity m , there will correspond an m -dimensional representation of S_n covering the same subspace [60, 67, 68]. The character table for S_4 is shown in Figure 2.

Table 2 Character table for the group S_4 which corresponds to the group of all permutations of the set $\{1, 2, 3, 4\}$. Each conjugacy class is characterised by the cycle structure of its permutations, where a cycle of length k corresponds to a sequence of k elements being permuted cyclically. The identity is represented by (I) , 2-cycles are represented by (12) and correspond to swapping any two elements. 3-cycles and 4-cycles are represented by (123) and (1234) , respectively. Disjoint cycles are those that affect different sets of elements and can be represented together, such as $(12)(34)$. There are five irreducible representations with their characters denoted by $\chi_1, \chi_2, \chi_3, \chi_4, \chi_5$.

Conjugacy Class	$C_{(I)}$	$C_{(12)}$	$C_{(12)(34)}$	$C_{(123)}$	$C_{(1234)}$
Number of Elements	1	6	3	8	6
χ_1	1	1	1	1	1
χ_2	1	-1	1	1	-1
χ_3	2	0	2	-1	0
χ_4	3	-1	-1	0	1
χ_5	3	1	-1	0	-1

If we utilise the irreducible representation projection procedure to project the state $|\mathbf{p}_1\rangle \otimes |\mathbf{p}_2\rangle \otimes |\mathbf{p}_3\rangle \otimes |\mathbf{p}_4\rangle$ to the subspace of irreducible representation $r = 3$, with characters χ_3 , then this corresponds to projecting to the basis states [60, 67, 68]

$$\begin{aligned} |d_1\rangle = \frac{\sqrt{3}}{6} & (2|0011\rangle + 2|1100\rangle - |0101\rangle \\ & - |1010\rangle - |0110\rangle - |1001\rangle), \end{aligned} \quad (106)$$

and

$$|d_2\rangle = \frac{1}{2}(|0101\rangle + |1010\rangle - |0110\rangle - |1001\rangle). \quad (107)$$

When writing the action of $(U \otimes U \otimes U \otimes U)$ in the Schur basis, as shown in Figure B.3, it can be seen that the above basis states $|d_1\rangle, |d_2\rangle$ are invariant under the action of $(U \otimes U \otimes U \otimes U)$ as they are in the subspace associated with the trivial representation of $SU(2)^{\otimes 4}$ [67, 68]. We are able to reach this space through projecting in S_4 due to Schur-Weyl duality, since the irreducible subspaces of S_4 and $SU(2)^{\otimes 4}$ are simultaneously block diagonalised. This means that we have effectively projected the quantum encoded point cloud state to a subspace which is invariant with respect to three-dimensional rotations of the point cloud. This is a desirable symmetry for point clouds, as they are naturally invariant to three-dimensional rotations.

In order to demonstrate this numerically, we show in Figure 10 that the rotationally invariant encoding introduced by this projection gives a constant overlap equal to unity when comparing two identical but rotated point clouds. This constant overlap

of unity is maintained as the degree of rotation is increased, demonstrating that the encoding is producing rotationally invariant encoded states. It is also demonstrated that, without applying this symmetry projection, a non-invariant encoding produces an overlap between identical but rotated point clouds that decreases as the magnitude of the rotation is increased. This is significant as it means that without a rotationally invariant encoding, the exact same point cloud, rotated by π radians, would produce a quantum state that appears completely different and will give zero overlap with the original orientation of the point cloud.

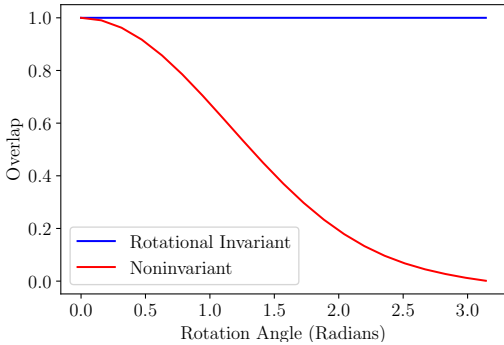


Fig. 10 The overlap between two identical Point Clouds that have been rotated about a random direction in three dimensions as the amount of rotation is increased, for the rotational invariant encoding and generic noninvariant encoding. To generate this plot, we randomly generated $n = 4$ points on a sphere of radius 1 to act as the point cloud. We then encoded the (θ, ϕ) radial coordinates of each point into a qubit using the specification of Equation 104. This results in an initial state $|P\rangle_{\text{init}} = |\mathbf{p}_1\rangle|\mathbf{p}_2\rangle|\mathbf{p}_3\rangle|\mathbf{p}_4\rangle$. We then repeat the procedure after the point cloud data is transformed by a three-dimensional rotation in random direction by some angle Θ to produce non-invariant state $|P\rangle_{\Theta}$. To generate rotationally invariant states $|P_{\text{rot}}\rangle_{\Theta}$ we apply the result in Theorem 3 to project $|P\rangle_{\Theta}$ states to the irreducible representation denoted by $r = 3$ as specified in Table 2, which via Schur-Weyl duality lie in the trivial representation subspace of $SU(2)^{\otimes 4}$ and are hence rotationally invariant under our data encoding set-up. This means we now have rotationally invariant encoded states $|P_{\text{rot}}\rangle_{\Theta}$ for all Θ values. The blue line plots the overlap $\langle P_{\text{init}} | P_{\text{rot}} \rangle_{\Theta}$ and the red line plots the overlap $\langle P_{\text{init}} | P \rangle_{\Theta}$ as the point cloud data rotation angle Θ is varied over $[0, \pi]$. As the overlap $\langle P_{\text{init}} | P_{\text{rot}} \rangle_{\Theta}$ is constant we therefore numerically confirm that projection to the irreducible representation denoted by $r = 3$ creates rotationally invariant states.

4.4 Symmetric Subspace Amplification

The rotationally invariant encoding discussed previously, as well as previous work on permutation invariant encodings [18] have been implemented in a binary fashion: the initial quantum state is either projected to a fully permutation invariant state or remains unchanged. Such an implementation significantly reduces the dimensionality of the encoding, yielding benefits in certain scenarios through improved generalisation of the model. This section explores the potential advantages of introducing a continuous spectrum of invariance with respect to some symmetry, rather than adhering to binary extremes, and investigates whether optimising this aspect as a hyperparameter could enhance classification performance in quantum machine learning (QML) models.

Recent studies suggest that permutation equivariant variational circuits may be classically tractable under specific conditions [49, 69], indicating that a drastic reduction in dimensionality might increase the likelihood of classical simulatability. This raises concerns that fully projecting to a polynomially sized subspace could render algorithms susceptible to classical simulation. To address these issues, we propose a novel approach that involves partially amplifying the portion of the quantum state into a given invariant space. Specifically, we will consider amplifying the permutation invariant subspace, although any irreducible subspace could be chosen. The projection to this amplified space is governed by a hyperparameter α which directly influences the expressibility of the encoding. This method provides enhanced control over training performance and facilitates the tuning of the model to achieve optimal results. For data types with inherent permutation symmetry, such as point cloud data, the optimal global classification function must also exhibit permutation invariance. However, the specific outcome of a QML model depends on the circuit architecture, classification protocol, and inherent limitations of QML models, suggesting that a purely permutation invariant QML algorithm may not necessarily be the closest to the global solution. We hypothesise that by incrementally adjusting the degree of permutation invariance in the model, we can converge towards a value that is closer to the true global optimum performance than is possible with an non-invariant, or fully permutation invariant model. This concept is illustrated in Figure 11.

The framework introduced previously allows the implementation of any linear combination of projections to an irreducible representation subspace with full control of the ratios of these projections. One can

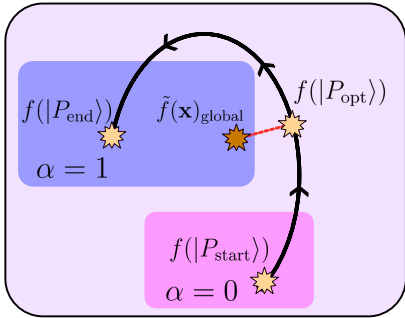


Fig. 11 Diagram providing a conceptual overview of the symmetric subspace amplification motivation. We start at $\alpha = 0$ with a state encoding $|P_{\text{start}}\rangle = \bigotimes_{i=1}^n |\mathbf{p}_i\rangle$ corresponding to an initial state without symmetry amplification, which is input to some classification model $f(\cdot)$. As α increases, the state moves through the solution space until finally we have a fully symmetric state at $\alpha = 1$ where the input state will be equal to $|P_{\text{end}}\rangle = \frac{1}{\sqrt{N}} \sum_{\sigma \in \mathcal{S}_n} |\mathbf{p}_{\sigma_1}\rangle |\mathbf{p}_{\sigma_2}\rangle \dots |\mathbf{p}_{\sigma_n}\rangle$ as initially proposed in [18]. If we are dealing with data that is known to be permutation symmetric, then the global optimal model for the input data $\tilde{f}(\mathbf{x})_{\text{global}}$ (which could be classical or quantum) must be within the fully permutation symmetric subspace of models. However, the precise model that yields the global optimum remains unknown and may not correspond to the function $f(\cdot)$ used in this particular case, suggesting that an intermediate value of α might align more closely with the global optimum than the fully symmetric projection at $\alpha = 1$. In the figure depicted, the red line illustrates the deviation between the global model solution and the nearest solution obtained at an intermediate value of α in which the input state is denoted $|P_{\text{opt}}\rangle$.

consider decomposing a state into its irreducible representation components, as shown in Figure 12 and gaining control over the relative ratios between the amplitude components, allowing them to be adjusted to suit the model and data.

$$|p\rangle = b \left| \begin{array}{|c|c|c|} \hline \square & \square & \square \\ \hline \end{array} \right\rangle \oplus c \left| \begin{array}{|c|c|} \hline \square & \square \\ \hline \end{array} \right\rangle \oplus d \left| \begin{array}{|c|c|} \hline \square & \square \\ \hline \end{array} \right\rangle$$

Fig. 12 A state can be viewed as a linear combination of its projection onto its irreducible representations. Utilising this projection algorithm we are able to change the relative weightings of b , c and d , effectively amplifying and reducing the portion of the original state that lies in the respective irreducible representation subspace.

Via the LCU framework we previous showed in Theorem 4 that it is possible to implement a projection onto a quantum state in the following form

$$\sum_r a_r \hat{P}_r |\psi\rangle, \quad (108)$$

where the a_r parameters can be controlled via the initial state of the ancilla qubits as

$$|c\rangle = \frac{1}{\Omega} \sum_{r=1}^R a_r n_r |b_r\rangle. \quad (109)$$

In order to implement the symmetric subspace amplification algorithm, one can define a parameter α that parameterises the amount of symmetry in the encoding. Then we can assign the following a_r values

$$a_r = \begin{cases} a_1 = 1 & \text{for } r = 1 \\ a_r = (1 - \alpha) & \text{for } r \neq 1 \end{cases} \quad (110)$$

Hence, the initial ancilla state will be of the form

$$|c\rangle = \frac{1}{\Omega} (n_1 |b_1\rangle + (1 - \alpha) \sum_{r=2}^R n_r |b_r\rangle). \quad (111)$$

The α term can be varied to adjust the amount of permutation symmetry. When $\alpha = 0$ this corresponds to an equal projection on all irreducible representations, since the resulting operation is an equal projection onto all subspaces (weighted by the dimension of the subspace) and hence will leave the state unchanged. In contrast, the case where $\alpha = 1$ will result in projection onto the symmetric subspace only. As α increases, this corresponds to continuously amplifying the portion of the state that lies in the symmetric subspace.

In order to investigate the potential of symmetric subspace amplification, we implemented the model proposed here utilising the aforementioned technique alongside Qiskit *statevector_simulator* [70]. This was used to encode point cloud data and perform classification on the sphere and torus point cloud dataset as specified in [18]. More details can be found in Appendix C.

We record the average test accuracy over 10 experiments for a given α and then vary α to see which value is optimal for the data. The results presented in Figure 13 illustrate that increasing the degree of symmetry yields the highest test accuracy at an intermediate value, demonstrating the potential advantage of this technique. Moreover, it is observed that while a fully symmetric projection ($\alpha = 1$) surpasses the performance of the non-symmetrised configuration ($\alpha = 0$), there is a significant reduction in dimensionality as

we approach a fully symmetric state. This reduction corresponds to projecting onto a polynomial size space for the case of symmetric subspaces [18]. A key concern with fully symmetric states is their potential for efficient classical simulation due to this polynomially sized space. In contrast, the technique of partial symmetrisation not only achieves higher accuracy but also resides in a higher-dimensional space, possibly making it more challenging to simulate classically.

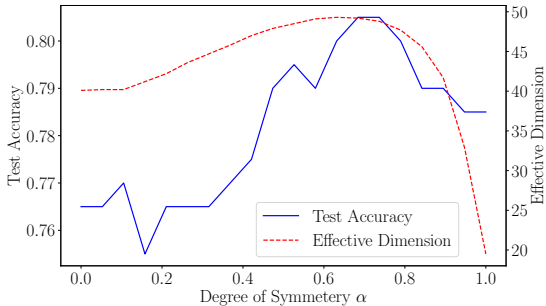


Fig. 13 Test accuracy and effective dimension as the degree of permutation symmetry is varied. Result is the average over 10 repeated experiments, each with 100 data points each of the sphere and torus classification dataset using quantum kernel estimation followed by a Support Vector Machine classification [18, 71, 72]. The effective dimension is found by explicitly calculating the higher dimensional encoding, performing principal component analysis, and calculating the amount of dimensions required to explain 95% of the variance of the dataset. We show that an intermediate value of permutation symmetry around $\alpha = 0.7$ results in the best performance for this classification.

5 Conclusion

In this study, we have demonstrated the applicability and flexibility of the Linear Combination of Unitaries method in enhancing Quantum Machine Learning architectures. Our work provides several implementations of classical machine learning structures within the quantum domain, achieving not only a foundational translation of these concepts but also demonstrating potential for computational advantages.

The implementation of Quantum ResNet demonstrates a promising avenue towards creating complex QML models that are resistant to classical simulation, and at the same time are capable of avoiding the trainability issues associated with barren plateaus. Although we highlight this potential in Section 2.4 it is still a question of further research as to finding bounds on this claim and characterising the cases in which this may or may not be useful in general. We

also demonstrated that by parameterising the strength of the residual connections through β_i terms, one can arbitrarily increase the lower bound probability of success of the LCU method. This provides an avenue to tackle the key problem of the LCU method, which is that the implementations can only be performed probabilistically.

We also demonstrated an implementation of quantum native average pooling layers commonly applied in convolutional neural networks. These layers have demonstrated success in classical techniques and therefore have the potential to improve quantum convolutional neural networks. Furthermore, we showed that given a quantum encoded image, the average pooling layers can be implemented without dependency on the size of the image due to the parallelism inherent in quantum circuits, offering potential computational speedups for large images.

Finally, we demonstrated an integration of irreducible representation projections into a quantum framework, allowing for the encoding of data symmetries directly into the quantum state, which has the potential to enhance the model’s generalisation capabilities across various data structures. This general irreducible subspace projection framework includes previous work regarding permutation invariant encodings for point clouds [18] as a special case, while in Section 4.3.2 we introduced a novel rotationally invariant encoding for point cloud data using the S_4 group. We further introduced in Section 4.4 a method of parameterising the amount of symmetry in an encoding as a tuneable hyperparameter. This added flexibility resulted in an improved performance for point cloud data when encoding an intermediate amount of permutation symmetry when compared to either a fully permutation invariant or noninvariant encoding. These were illustrative examples of how the framework could be utilised and there could be many possible symmetries and datasets for which this framework could be similarly adapted and optimised.

As the field of quantum computing continues to mature, the methods and frameworks presented here offer promising avenues for developing more sophisticated quantum algorithms that leverage both the computational benefits of quantum mechanics and the established successes of classical machine learning architectures. By utilising LCU methods we have shown non-unitary operations can be applied in a QML setting; this research not only extends the theoretical possibilities and flexibility of QML algorithms but also provides practical frameworks for their application, setting the stage for further evolution of quantum machine learning models.

Author Contributions

J. Heredge envisaged the project, initially focused on irreducible subspace projections, with M. Sevir and L. Hollenberg as an extension of their previous work [18]. J. Heredge devised the ResNet and Average Pooling layers applications. The theorems and numerical simulations were developed by J. Heredge with the help of M. West. M. Sevir and L. Hollenberg supervised the overall project. All authors contributed in reviewing the manuscript.

Acknowledgements

This research was supported by the Australian Research Council from grant DP210102831. J. Heredge acknowledges the support of the Australian Government Research Training Program Scholarship and the support of the N.D. Goldsworthy Scholarship. This work was supported by the University of Melbourne through the establishment of an IBM Quantum Network Hub at the University. We thank Dougal Davis for early discussions on representation theory that helped aid the development of the irreducible subspace projection work. We also thank Giulio Crognaletti for discussions on current quantum ResNet literature.

Appendix A Conjugacy Class Implementation

In the implementation of irreducible subspace projections detailed in Section 4, an operator $\hat{\chi}$ was required that contained the character of every element in the group G . This meant that the dimension of the matrix scaled with $|G|$, which can be problematic for some groups, such as the permutation group S_n where $|S_n| = n!$. To tackle this, in this section we will consider a unitary operator $\tilde{\chi}$ that contains the character for each conjugacy class in the group, with additional ancilla qubit registers per conjugacy class prepared in an equal superposition that then acts to distribute these characters to the corresponding group elements. This effectively only requires encoding the character table of the group into a unitary operator, and hence $\tilde{\chi}$ scales with the number of conjugacy classes of G . This has the potential to drastically reduce the size of the unitary that must be applied, at the expense of requiring additional ancilla qubits. We show that utilising this circuit structure recreates the result of Theorem 4 and is therefore a valid alternative approach.

The character orthogonality theorem [64] stated previously in Equation 86 relates to a sum over all the

Table A1 Character table for the group S_3 . There are three irreducible representations with their characters denoted by χ_1, χ_2, χ_3 . The conjugacy classes of S_3 are $C_{(I)} = \{I\}$, $C_{(12)} = \{\sigma_{12}, \sigma_{13}, \sigma_{23}\}$ and $C_{(123)} = \{\sigma_{231}, \sigma_{312}\}$.

Conjugacy Class ν_i	$C_{(I)}$	$C_{(12)}$	$C_{(123)}$
Number of Elements d_{ν_i}	1	3	2
χ_1	1	1	1
χ_2	2	0	-1
χ_3	1	-1	1

elements of the group. As the character is the same for all elements in a conjugacy class, this can be adjusted to a sum over all conjugacy classes $\nu_i \in \mathcal{C}$ by introducing a term $d_{\nu_i} = |\nu_i|$ that represents the number of group elements in the conjugacy class ν_i . Therefore, the character orthogonality theorem can be written

$$\frac{1}{|G|} \sum_{\nu_i \in \mathcal{C}} d_{\nu_i} \chi_j(\nu_i) \chi_k(\nu_i)^* = \delta_{j,k}. \quad (\text{A1})$$

Therefore, to create a matrix with orthonormal columns (to ensure $\tilde{\chi}$ is unitary) the characters for a conjugacy class ν must be weighted by square root of the number of elements in the conjugacy class $\sqrt{d_{\nu_i}}$. Hence, we require that

$$\tilde{\chi}|r\rangle = \frac{1}{\sqrt{|G|}} \sum_{\nu_i \in \mathcal{C}} \sqrt{d_{\nu_i}} \chi_r(\nu_i)^* |\nu_i\rangle, \quad (\text{A2})$$

where in this case the conjugacy classes $\nu_i \in \mathcal{C}$ are labelling the basis states $|\nu_i\rangle \equiv |b_i\rangle$ defined as $\{|b_j\rangle\}_{j \in [1, 2^k]} \in (\mathbb{C}^2)^{\otimes k}$ the basis states of the 2^k dimensional Hilbert space for the k qubit ancilla register denoted by $\mathcal{H} = (\mathbb{C}^2)^{\otimes k}$. These can be taken to be the computational basis states.

If we consider S_3 with its character table given in Table A1 then we see that in this case the appropriate unitary matrix to be constructed would be

$$\tilde{\chi} = \frac{1}{\sqrt{6}} \begin{bmatrix} 1 & 2 & 1 & 0 \\ \sqrt{3} & 0 & -\sqrt{3} & 0 \\ \sqrt{2} & -\sqrt{2} & \sqrt{2} & 0 \\ 0 & 0 & 0 & 1 \end{bmatrix} \quad (\text{A3})$$

This successfully allows for the construction of a unitary matrix $\tilde{\chi}$ that scales in size with the number of conjugacy classes as opposed to the number of group elements. We therefore have satisfied the constraint that $\tilde{\chi}$ is unitary and can be implemented on a quantum device.

Similarly to the main text, the first step is the pre-initialisation of the ancilla qubits to some combination of states that index the different irreducible

representations

$$\hat{\gamma}|b_1\rangle|\psi\rangle = \frac{1}{\Omega} \sum_{r=1}^R a_r n_r |b_r\rangle|\psi\rangle, \quad (\text{A4})$$

where $|b_1\rangle$ is the initial state of the ancilla qubit register, usually assumed to be $|0\rangle^{\otimes k}$. By applying $\tilde{\chi}$ to this pre-initialised ancilla state, one can write

$$\begin{aligned} \tilde{\chi}\hat{\gamma}|b_1\rangle|\psi\rangle &= \tilde{\chi} \frac{1}{\Omega} \sum_{r=1}^R a_r n_r |b_r\rangle|\psi\rangle \\ &= \frac{1}{\Omega\sqrt{|G|}} \sum_{r=1}^R a_r n_r \sum_{\nu_i \in \mathcal{C}} \sqrt{d_{\nu_i}} \chi_r(\nu_i)^* |\nu_i\rangle|\psi\rangle, \end{aligned} \quad (\text{A5})$$

where as previously stated $|\nu_i\rangle \equiv |b_i\rangle$ are the same basis states, usually taken to be the computational basis states, but we have switched from $|b_r\rangle$ being indexed by the irreducible representation r , to the basis states being labelled by the conjugacy class ν_i . This contrasts to $\hat{\chi}$ in the main text, where the group elements label the ancilla states. After application of $\tilde{\chi}$ the ancilla qubits now have basis states corresponding to the conjugacy classes $|\nu_i\rangle$. The selection operator requires the creation of additional qubit ancilla registers, denoted by $|\omega_{\nu_i}\rangle$, for each conjugacy class which are encoded into an equal superposition of $d_{\nu_i} = |\nu_i|$ states

$$|\omega_{\nu_i}\rangle = \frac{1}{\sqrt{d_{\nu_i}}} \sum_{l_{\nu_i}=1}^{d_{\nu_i}} |l_{\nu_i}\rangle, \quad (\text{A6})$$

where $|l_{\nu_i}\rangle$ are basis states $\{|l_{\nu_i}\rangle\} \in (\mathbb{C}^2)^{\otimes k_{\nu_i}}$ of the $2^{k_{\nu_i}}$ dimensional Hilbert space for the k_{ν_i} qubit ancilla register $|\omega_{\nu_i}\rangle$ that is encoded on k_{ν_i} qubits, which can be taken to be the computational basis states. The groups elements l_{ν_i} that are contained in the conjugacy class ν_i now label the basis states in register $|\omega_{\nu_i}\rangle$. Each register has the requirement $k_{\nu_i} \geq \log(d_{\nu_i})$ to ensure that there are sufficient qubits in the register such that each element in ν_i has a corresponding basis state $|l_{\nu_i}\rangle$.

Overall the operations up to this point can be written as

$$\begin{aligned} &\bigotimes_{\nu_i'} |\omega_{\nu_i'}\rangle \otimes \tilde{\chi}\hat{\gamma}|b_1\rangle \otimes |\psi\rangle \\ &= \frac{1}{\Omega\sqrt{|G|}} \left(\left(\bigotimes_{\nu_i'} \frac{1}{\sqrt{d_{\nu_i'}}} \sum_{l_{\nu_i'}=1}^{d_{\nu_i'}} |l_{\nu_i'}\rangle \right) \right. \\ &\quad \left. \otimes \sum_{r=1}^R a_r n_r \sum_{\nu_i \in \mathcal{C}} \sqrt{d_{\nu_i}} \chi_r(\nu_i)^* |\nu_i\rangle|\psi\rangle \right). \end{aligned} \quad (\text{A7})$$

The controlled operations are performed similarly to the main text, except in this case the group element $g \in G$ is indexed by both ν_i which determines the conjugacy class and l_{ν_i} which indexes the element within the given conjugacy class. In this case $S_{\text{SELECT}} \equiv \hat{S}$ will be controlled by both the conjugacy class state $|\nu_i\rangle$ and the element selector within the conjugacy class $|l_{\nu_i}\rangle$ of the register $|\omega_{\nu_i}\rangle$ associated with the conjugacy class ν_i . The action of this selection operator can be defined as

$$\hat{S}|l_{\nu_i}\rangle|\nu_i\rangle|\psi\rangle = |l_{\nu_i}\rangle|\nu_i\rangle U_{\nu_i, l_{\nu_i}} |\psi\rangle, \quad (\text{A8})$$

which is implemented by each unitary $U_{\nu_i, l_{\nu_i}}$ being controlled by both the $|l_{\nu_i}\rangle$ and $|\nu_i\rangle$ states. Applying this operator one can see the effect is

$$\begin{aligned} &\hat{S} \left(\bigotimes_{\nu_i'} |\omega_{\nu_i'}\rangle \otimes \tilde{\chi}\hat{\gamma}|b_1\rangle \otimes |\psi\rangle \right) \\ &= \frac{1}{\Omega\sqrt{|G|}} \left(\sum_{\nu_i} \left(\bigotimes_{\nu_i' \neq \nu_i} \frac{1}{\sqrt{d_{\nu_i'}}} \sum_{l_{\nu_i'}=1}^{d_{\nu_i'}} |l_{\nu_i'}\rangle \right) \right. \\ &\quad \left. \otimes \sum_{r=1}^R \sum_{l_{\nu_i}=1}^{d_{\nu_i}} \frac{a_r n_r}{\sqrt{d_{\nu_i}}} \chi_r(\nu_i)^* |l_{\nu_i}\rangle|\nu_i\rangle U_{\nu_i, l_{\nu_i}} |\psi\rangle \right) \\ &= \sum_{\nu_i} \bigotimes_{\nu_i' \neq \nu_i} |\omega_{\nu_i'}\rangle \sum_{r=1}^R \sum_{l_{\nu_i}=1}^{d_{\nu_i}} \frac{a_r n_r \chi_r(\nu_i)^*}{\Omega\sqrt{d_{\nu_i}|G|}} |l_{\nu_i}\rangle|\nu_i\rangle \\ &\quad \otimes U_{\nu_i, l_{\nu_i}} |\psi\rangle, \end{aligned} \quad (\text{A9})$$

where we are being flexible with the precise positioning in the tensor product of the unused registers $|\omega_{\nu_i' \neq \nu_i}\rangle$ for each ν_i' term for the sake of readability. The registers $|\omega_{\nu_i}\rangle$ that contain the states $|l_{\nu_i}\rangle$ will in fact no longer be used in the circuit and can be ignored. They have performed their role in ensuring that the correct $U_{\nu_i, l_{\nu_i}}$ was applied to the state $|\psi\rangle$. This means we can simplify the expression to

$$\begin{aligned} &\hat{S} \left(\bigotimes_{\nu_i'} |\omega_{\nu_i'}\rangle \otimes \tilde{\chi}\hat{\gamma}|b_1\rangle \otimes |\psi\rangle \right) \\ &= \sum_{\nu_i} \sum_{r=1}^R \sum_{l_{\nu_i}=1}^{d_{\nu_i}} \frac{a_r n_r \chi_r(\nu_i)^*}{\Omega\sqrt{d_{\nu_i}|G|}} |l_{\nu_i}\rangle|\nu_i\rangle U_{\nu_i, l_{\nu_i}} |\psi\rangle. \end{aligned} \quad (\text{A10})$$

The final steps consist of applying $\tilde{\chi}^\dagger$ and measuring the conjugacy class $|\nu_i\rangle$ ancillas to be in the initial state $|b_1\rangle$. Due to the fact that the state $|b_1\rangle$, which is commonly assumed to be $|0\rangle^{\otimes k}$, is used to index the first representation, we can write

$$\langle b_1 | \tilde{\chi} = \frac{1}{\sqrt{|G|}} \sum_{\nu_i \in \mathcal{C}} \sqrt{d_{\nu_i}} \chi_1(\nu_i) \langle \nu_i |. \quad (\text{A11})$$

where noticeably $\chi_1(\nu_i) = 1, \forall \nu_i$ due to the fact that we are free to define $r = 1$ to always correspond to the trivial representation when constructing $\tilde{\chi}$. Applying this operator to the conjugacy class ancilla qubits in the circuit therefore results in

$$\begin{aligned} & \left(\langle b_1 | \tilde{\chi} \right) \cdot \left(\hat{S} \left(\bigotimes_{\nu_i'} |\omega_{\nu_i'}\rangle \otimes \tilde{\chi} \hat{\gamma} |b_1\rangle \otimes |\psi\rangle \right) \right) \\ &= \frac{1}{\Omega'} \sum_{\nu_i} \sum_{r=1}^R \sum_{l_{\nu_i}=1}^{d_{\nu_i}} a_r \frac{n_r}{|G|} \chi_r(\nu_i)^* U_{\nu_i, l_{\nu_i}} |\psi\rangle, \end{aligned} \quad (\text{A12})$$

where $\Omega' = \Omega \sqrt{\pi_S}$ is the normalisation constant of the final state. Due to the fact that conjugacy classes partition the group G , the labels of the conjugacy class ν_i along with the labels of the elements within each conjugacy class l_{ν_i} will uniquely index each group element. In addition, all elements in the same conjugacy class have the same character i.e., $\chi_r(g_1) = \chi_r(g_2)$ for $g_1, g_2 \in \nu_i$. Hence, we can relabel the above expression in terms of group elements g , rather than ν_i and l_{ν_i} , to explicitly see that it can be written as

$$\frac{1}{\Omega} \sum_{r=1}^R a_r \frac{n_r}{|G|} \sum_{g \in G} \chi_r(g)^* U_g |\psi\rangle. \quad (\text{A13})$$

This is the precise form of Equation 81 in Theorem 4. Hence, we have provided another framework that satisfies the theorem in the main text. As the final step consisted only of reordering the indexing, it follows that probability of success π_S will be the same as in the main text.

The dimension of $\tilde{\chi}$ scales with the number of conjugacy classes of the group G as opposed to $\tilde{\chi}$ in the main text, which scales with the number of elements in the group. This means that $\tilde{\chi}$ could potentially be much easier to implement than $\tilde{\chi}$. However, a caveat is that an additional ancillary qubit register $|\omega_{\nu_i}\rangle$ is required for each conjugacy class ν_i , where each register will contain a number of qubits of the order $\mathcal{O}(\log(d_{\nu_i}))$. This presents a trade-off between unitary implementation difficulty and the number of ancilla qubits required. The true difficulty in implementing either unitary will ultimately depend on the group, but we provide both of these general techniques as possible starting points for future implementations.

Appendix B Rotational Invariance via Schur-Weyl

In this section, we demonstrate how certain irreducible representations of S_n could correspond to rotationally invariant encoding states when using the encoding specified in Section 4.3.2. Following the work and explanations of [60, 67] and in particular the thesis [68] we reproduce an overview of Schur-Weyl duality and the concept of the Schur basis and add discussion at points linking this to how certain irreducible representation subspaces would correspond to rotationally invariant point cloud encodings in the case considered in Equation 104.

B.1 Introduction to Schur Transforms

The rotational invariant point cloud encoding we propose in Section 4.3.2 relies on a property of the probabilistic irreducible subspace projection circuit when considering the group S_n , which in effect performs a projection to basis states of the Schur basis. Circuits that implement quantum Schur transforms have previously been introduced, such as those that implement them through the unitary group by iteratively applying the Clebsch-Gordan transforms [73] and alternative methods that implement it by considering the action of the symmetric group using quantum Fourier transforms [74]. Indeed, further investigation on whether the use of these existing algorithms could be adapted to more efficiently refine our procedure would be an interesting further research direction, as our implementation derives from the most general case of Theorem 4 which applies to any group G and therefore may not be the most efficient in practice.

The Schur transform is related to the concept of Schur-Weyl duality. In general, we can consider n qudits of dimension d inside a vector space $(\mathbb{C}^d)^{\otimes n}$ with a computational basis written as $|i_1\rangle \otimes |i_2\rangle \otimes \dots \otimes |i_n\rangle$. There are two representations on this space that are related to each other by Schur-Weyl duality. One of the representations is that of the Symmetric Group S_n , whose elements consist of all possible permutations of n objects. The representation of S_n on this vector space would simply consist of permuting the qudits. For a given group element $\sigma \in S_n$ one can write the action of the representation $P(\sigma)$ on this vector space as

$$P(\sigma) |i_1\rangle \otimes \dots \otimes |i_n\rangle = |i_{\sigma^{-1}(1)}\rangle \otimes \dots \otimes |i_{\sigma^{-1}(n)}\rangle. \quad (\text{B14})$$

Hence, each $\sigma \in S_n$ simply corresponds to a different permutation of the n qudits.

The second group to consider is the group of all $d \times d$ unitary operators $U \in \mathcal{U}_d$. As each qudit forms a d -dimensional vector, we see that the natural representation $Q(U)$ of the group \mathcal{U}_d acting on the vector space $(\mathbb{C}^d)^{\otimes n}$ would correspond to the n -fold product action, where the same U is applied to each qudit. This can be written as

$$Q(U)|i_1\rangle \otimes \dots \otimes |i_n\rangle = U|i_1\rangle \otimes \dots \otimes U|i_n\rangle. \quad (\text{B15})$$

The two actions $Q(U)$ and $P(\sigma)$ are fully reducible and hence can be written as a direct sum of their irreducible representations

$$P(\sigma) \rightarrow \bigoplus_{\alpha} \mathbf{I}_{n_{\alpha}} \otimes p_{\alpha}(\sigma), \quad (\text{B16})$$

$$Q(U) \rightarrow \bigoplus_{\beta} \mathbf{I}_{m_{\beta}} \otimes q_{\beta}(U). \quad (\text{B17})$$

Note that the actions $P(\sigma)$ and $Q(U)$ commute with each other. The Schur-Weyl duality therefore states that there exists a basis which simultaneously decomposes the action of $P(\sigma)$ and $Q(U)$ into irreducible representations as

$$Q(U)P(\sigma) \rightarrow \bigoplus_{\lambda} q_{\lambda}(U)p_{\lambda}(\sigma). \quad (\text{B18})$$

We can write this Schur basis as $|\lambda\rangle|q_{\lambda}\rangle|p_{\lambda}\rangle_{Sch}$ which decomposes the action of $P(\sigma)$ and $Q(U)$ as

$$Q(U)|\lambda\rangle|q_{\lambda}\rangle|p_{\lambda}\rangle_{Sch} = |\lambda\rangle(q_{\lambda}^d(U)|q_{\lambda}\rangle)|p_{\lambda}\rangle_{Sch}, \quad (\text{B19})$$

$$P(\sigma)|\lambda\rangle|q_{\lambda}\rangle|p_{\lambda}\rangle_{Sch} = |\lambda\rangle|q_{\lambda}\rangle(p_{\lambda}(\sigma)|p_{\lambda}\rangle)_{Sch}. \quad (\text{B20})$$

This action will decompose the vector space $(\mathbb{C}^d)^{\otimes n}$ as

$$(\mathbb{C}^d)^{\otimes n} \rightarrow \bigoplus_{\lambda \in \Lambda} \mathcal{Q}_{\lambda}^d \otimes \mathcal{P}_{\lambda}. \quad (\text{B21})$$

Note that since these subspaces \mathcal{Q}_{λ}^d and \mathcal{P}_{λ} are irreducible, the action of the representation $Q(U)$ or $P(\sigma)$ on a vector in spaces will keep the vector in that space. We will focus on building the Schur basis through considering the action of $P(\sigma)$ for $\forall \sigma \in S_n$.

B.2 Rotational Invariance for Two Points is Trivial

If we wish to find states that are rotationally invariant as we rotate points in a 3 dimensional point cloud, we should first consider what this means on the point cloud data. Each point can be represented by a vector in \mathcal{R}^3 . If the entire point cloud is rotated, this amounts

to every point being transformed by the same rotation, which is equivalent to applying a rotation matrix from the group $SO(3)$ to each point.

A natural way we choose to represent rotations of points in a quantum encoding is as rotations on the Bloch sphere representation of a qubit as was detailed in Section 4.3.2. This is further motivated by the fact that $SU(2)$ is the double cover of $SO(3)$, which means that every point in $SO(3)$ corresponds to two points in $SU(2)$, which means that we can use $SU(2)$ to model rotations in three-dimensional space classified by $SO(3)$. To produce an encoding like this, we simply need to apply the parameterised rotation gates $R_x(\theta)$ and $R_z(\phi)$ to an initial $|0\rangle$ state, where (θ, ϕ) are the angle coordinates of a point in radial coordinates. We are now left with the angular direction of the point represented in the Bloch sphere of a single qubit. If we do this for all n points in the point cloud, we will have n qubits. A rotation of the entire point cloud can now be represented by the application of any $SU(2)$ unitary to every qubit simultaneously. This is a tensor representation of the $SU(2)$ group and can be written explicitly as $\bigotimes_{i=1}^n U$ for $U \in SU(2)$.

To further study this, we shall resort to the case consisting of only two points $n = 2$. We again follow standard explanations from reference texts [60, 67, 68] while relating these points back to the rotationally invariant encoding we propose throughout the discussion. In this case rotation of the point cloud corresponds to applying the representation $U \otimes U$; $U \in SU(2)$, to the two qubits. Note that this construction commutes with the SWAP operator $[U \otimes U, \text{SWAP}] = 0$, where SWAP corresponds to permuting the two qubits. This fact means that any eigenvectors of $U \otimes U$ with eigenvalue λ must also be an eigenvector of SWAP with eigenvalue λ .

If we consider two qubits such that $V = (\mathbb{C}^2)^{\otimes 2}$ and the group S_2 then a natural representation on two qubits would be $\{\mathbb{I}, \text{SWAP}\}$. If we change from the computational basis to the Schur basis $\{|00\rangle, \frac{1}{\sqrt{2}}(|01\rangle + |10\rangle), |11\rangle, \frac{1}{\sqrt{2}}(|01\rangle - |10\rangle)\}$, then we can see that this is a basis of eigenvectors for the SWAP operator that is completely diagonalised in this basis. We can show this explicitly as

$$\begin{aligned} \text{SWAP}|00\rangle &= |00\rangle, \\ \text{SWAP}\frac{1}{\sqrt{2}}(|01\rangle + |10\rangle) &= \frac{1}{\sqrt{2}}(|01\rangle + |10\rangle), \\ \text{SWAP}|11\rangle &= |11\rangle, \\ \text{SWAP}\frac{1}{\sqrt{2}}(|01\rangle - |10\rangle) &= -\frac{1}{\sqrt{2}}(|01\rangle - |10\rangle). \end{aligned} \quad (\text{B22})$$

As both $\{\mathbb{I}, \text{SWAP}\}$ have the same action when applied to the basis states $\{|00\rangle, |11\rangle, \frac{1}{\sqrt{2}}(|01\rangle + |10\rangle)\}$,

this means it corresponds to the trivial representation $\mathbf{1}$ of S_2 . The action on this subspace leaves states unchanged and hence they have an eigenvalue of 1. The action of SWAP when applied to the basis state $\{|01\rangle - |10\rangle\}$, leads to a sign flip (eigenvalue of -1) which is therefore denoted as the **sign** representation of S_2 , where the sign of the state gets flipped by SWAP and remains unchanged under \mathbb{I} .

We can simultaneously block diagonalise $U \otimes U$ and SWAP as they both commute $[U \otimes U, SWAP] = 0$. Hence $U \otimes U$ is block diagonalised in this basis. This means that if we have a state in the space spanned by $\{|00\rangle, \frac{1}{\sqrt{2}}(|01\rangle + |10\rangle), |11\rangle\}$ that it will in this space under the operation of $U \otimes U$. It is possible to identify for $U \otimes U$ a symmetric eigenspace, denoted $\text{Sym}^2(\mathbb{C}^2)$, with eigenvalue $\lambda_{\text{sym}} = 1$ along with an anti-symmetric eigenspace, denoted $\wedge(\mathbb{C}^2)$, with an eigenvalue $\lambda_{\text{ant}} = -1$.

If we want to find a state that is invariant under S_2 , which in this case corresponds to permuting the order of the qubits, then the state needs to be in the eigenspace of the trivial representation of S_2 , this corresponds to the state formed with the basis $\{|00\rangle, |01\rangle + |10\rangle, |11\rangle\}$, as in this basis both \mathbb{I} and SWAP both leave the state unchanged, hence the state is permutation invariant. Projections to this subspace is how permutation invariant encodings are performed, as initially suggested in [18].

However, while the symmetric space is closed under the action $U \otimes U$, the application of the unitaries will still change the state. If we have a unitary matrix given by

$$U = \begin{pmatrix} a & -b^* \\ b & a^* \end{pmatrix}, \quad (\text{B23})$$

where $|a|^2 + |b|^2 = 1$. If one applies a Schur transform to $U \otimes U$ which transforms it into the basis described previously it has been shown that it takes a block diagonal form [67, 68]

$$\text{Sch}(U \otimes U)\text{Sch}^\dagger = \begin{pmatrix} a^2 & -\sqrt{2}ab^* & (b^*)^2 & 0 \\ \sqrt{2}ab & |a|^2 - |b|^2 & -\sqrt{2}a^*b^* & 0 \\ b^2 & \sqrt{2}a^*b & (a^*)^2 & 0 \\ 0 & 0 & 0 & 1 \end{pmatrix} \quad (\text{B24})$$

and the SWAP operator can be written as

$$\text{Sch}(\text{SWAP})\text{Sch}^\dagger = \begin{pmatrix} 1 & 0 & 0 & 0 \\ 0 & 1 & 0 & 0 \\ 0 & 0 & 1 & 0 \\ 0 & 0 & 0 & -1 \end{pmatrix} \quad (\text{B25})$$

The symmetric subspace consists of the upper left block. $U \otimes U$ will transform the state, but keep it within the symmetric subspace. This also means that any variational circuit of the form $U \otimes U$ will similarly

keep the state symmetric. This is the intuition behind geometric QML techniques in which variational layers can be constructed, such as $U \otimes U$ in this case, that preserve the symmetry of the state they act on while still allowing variational parameters to be adjusted [33]. Although in this work we do not consider creating variational circuits that preserve symmetry, instead we focus on projecting quantum encoded states to irreducible subspaces, which strictly enforces the symmetry invariance in the model as all information in the quantum state is deleted except the portion lying in the chosen irreducible subspace before the training and classification step are considered. It is important to note that the multiplicity of the subspace of S_n corresponds to the dimension of the representation of $U \otimes U$ in that subspace and vice versa.

If we require a state to be rotationally invariant using the encoding previously described, we require that the state lies in the subspace corresponding to the trivial representation of $SU(2)$, as under the trivial representation the state will be unchanged by the action $U \otimes U$. In the case $n = 2$, this would correspond to the basis consisting of a single eigenvector $\frac{1}{\sqrt{2}}(|01\rangle - |10\rangle)$. This is now the trivial representation for $SU(2)$ but corresponds to the **sign** representation in S_2 . This means that the state is invariant under $SU(2)$ but the SWAP operator changes its sign, hence it is not invariant under permutation. As the dimension and multiplicity of the space is 1, the only normalised state that can exist in this space would be the state $\frac{1}{\sqrt{2}}(|01\rangle - |10\rangle)$. Therefore, any projection onto the antisymmetric space for $n = 2$ would correspond to projection to the state $\frac{1}{\sqrt{2}}(|01\rangle - |10\rangle)$, which would provide rotational invariance, but result in a trivial encoding as all information about the data would be lost. Hence we show that as $U \otimes U$ and S_2 can be simultaneously block diagonalised, that we can perform projections for S_2 that take the state to a space that is the trivial representation of $U \otimes U$ and is therefore a rotationally invariant state. Note that it would not be possible in this set-up to have a state which is both permutation invariant and rotationally invariant, as they correspond to orthogonal irreducible subspaces.

We also note that if we consider the case where one attempts to create a equivariant variational quantum model that is rotationally invariant in a similar manner to how permutation equivariant models are created in this context, then the variational layer would have to be composed of SWAP gates. These clearly do not have the ability to be parameterised by any variational parameters and therefore it is not possible to create such a variational circuit if strictly following the line of reasoning presented here, although they could be implemented with a different

projecting onto the $r = 3$ representation of S_4 (as specified in Table 2) using the projection circuit proposed in Section 4, the quantum input state $|\psi\rangle$ will be projected onto some state $|\psi_{\text{rot}}\rangle = \lambda_1|d_1\rangle + \lambda_2|d_2\rangle$. In this case there are now two basis states that can be used. However, due to the normalisation constraint $|\lambda_1|^2 + |\lambda_2|^2 = 1$ the effective dimension is reduced to be equal to 1 overall. This means that at least some information from the original input state is retained when the projection is performed and is therefore a non-trivial example, although effective projection to a 1-dimensional space may be too great a dimensionality reduction in practice.

In general, if it is possible to calculate the multiplicity of the trivial representation of dimension 1 of $SU(2)^{\otimes n}$ to be m_{SU} , then by Schur-Weyl duality there exists an irreducible subspace of S_n of dimension m_{SU} and multiplicity of 1. Projecting to this subspace will therefore result in reducing the dimensionality of the encoded data to $m_{SU} - 1$, after considering the normalisation condition. We provide this rotationally invariant encoding as an example to demonstrate how the irreducible subspace projection circuit could be utilised for point cloud data, complementing previous work on permutation invariant encodings of point cloud data [18]. It may be the case that this is not feasible or useful for $n > 4$ and such investigations could be subject to further research. However, the main motivation was to provide an additional example of how the projection framework could be used to encode symmetry in a model. In general, the irreducible subspace projection framework we introduced can be used for any representation of any finite compact group G along with any encoding procedure for $|\psi\rangle$ and hence there exists ample flexibility for application to a wide array of problems beyond those mentioned as examples in this work.

Appendix C Point Cloud Numeric Details

This section specifies the details of the numerical results reported in Section 4.4. To generate the data, $n = 3$ points were sampled from the surface of a shape, either a sphere or a torus as originally used in [18], to create point clouds. The process is repeated with an equal amount of point clouds from each shape until the desired number of total samples is reached. These are split into training sets (80%) and testing sets (20%). We evaluated the performance of the model on the test set and averaged the accuracy in 10 experiments in which a newly generated dataset is used each time. Both the sphere and torus are centred at the origin,

with the torus scaled to match the sphere’s average point magnitude. All data is normalised between $-\frac{\pi}{2}$ and $\frac{\pi}{2}$ to be encoded as rotation angles.

To encode a point cloud, each point $\mathbf{p}_i = (x_i, y_i, z_i)$ is first encoded into a two qubit quantum state $|\mathbf{p}_i\rangle$ using two repeated layers of the encoding circuit shown in Figure C2. Then the corresponding statevector is found using Qiskit `statevector_simulator` [70]. From here we can write the entire point cloud as $|P\rangle = |\mathbf{p}_1\rangle \otimes |\mathbf{p}_2\rangle \otimes |\mathbf{p}_3\rangle$. In order to perform the simulations we then found the projection of $|P\rangle$ onto each irreducible subspace classically utilising the result specified in Theorem 3 and the character table for S_3 . From here the a_r parameters specified in Equation 110 are used to produce the correct linear combination of projections and arrive at the partially symmetric subspace amplified state $|P\rangle_\alpha$, with the amount of symmetry parameterised by α . We then implement a quantum support vector machine classification by calculating the inner product between the data points to form a kernel matrix, which is then input to a classical support vector machine for the final classification [18, 71]. We recorded the average test accuracy over 10 experiments for a given α and then repeated with different α values and plotted the results to see which value of α is optimal for the data.

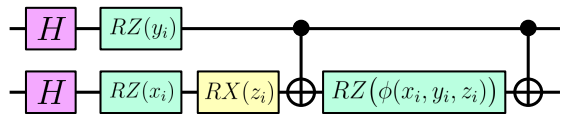


Fig. C2 One layer of the encoding circuit used to encode an individual point $\mathbf{p}_i = (x_i, y_i, z_i)$ in the symmetric subspace amplification model. The function $\phi(x_i, y_i, z_i) = \frac{2}{\pi^2}(\pi - x_i)(\pi - y_i)(\pi - z_i)$ means the entanglement of the state is dependent on some polynomial of all input variables. To generate the encoded state $|\mathbf{p}_i\rangle$ two repeated layers of this circuit are used [71, 72].

Appendix D Dimensionality Reduction in Pooling Layers

Regarding the average pooling layers implemented in this work in Section 3, it is crucial to understand that we have confined our operations to averaging quantum states across image translations. Notably, binary addition operates cyclically, where adding 1 to the highest value loops back to the lowest value, meaning our tiling would wrap around the edges of the image to perform the averaging. This may be an undesirable effect, unless the image has some periodic feature. It is

also the case that the average pooling described does not provide any dimensionality reduction, as we can calculate the pooling window average for every pixel at no additional computational cost.

To perform the dimensionality reduction, and to prevent the image being treated as periodic, one method could involve deleting any states in which $x_i > N - L$ or $y_j > N - L$ after the averaging part of the pooling layer is implemented by implementing

$$|x_i\rangle|y_j\rangle \rightarrow \text{DELETE if } x_i \text{ or } y_j > N - L. \quad (\text{D28})$$

To perform this without any a priori information of the data or architecture, one can define the $F_{\text{FLAG},x}$ and $F_{\text{FLAG},y}$ operators alongside two ancilla flag qubits, one for the x and y flags, respectively.

$$\begin{aligned} F_{\text{FLAG},x}|x_i\rangle|y_j\rangle|0\rangle_x|0\rangle_y \\ = \begin{cases} |x_i\rangle|y_j\rangle|0\rangle_x|0\rangle_y & \text{if } x_j \leq N - L \\ |x_i\rangle|y_j\rangle|1\rangle_x|0\rangle_y & \text{if } x_j > N - L \end{cases} \end{aligned} \quad (\text{D29})$$

and

$$\begin{aligned} F_{\text{FLAG},y}|x_i\rangle|y_j\rangle|0\rangle_x|0\rangle_y \\ = \begin{cases} |x_i\rangle|y_j\rangle|0\rangle_x|0\rangle_y & \text{if } y_j \leq N - L \\ |x_i\rangle|y_j\rangle|0\rangle_x|1\rangle_y & \text{if } y_j > N - L \end{cases} \end{aligned} \quad (\text{D30})$$

One can now effectively remove unwanted states to reduce the dimensionality by measuring the ancilla warning qubits and disregarding results unless $|0\rangle_x|0\rangle_y$ is measured. This will delete any states in which the average pooling layer will have wrapped around the sides of the image.

Clearly as this is a probabilistic procedure we expect that significantly more efficient implementations are possible depending on the exact specifics of the problem. For example, if it is known that some of the most significant qubits correspond to pixels that should not be used, then they can simply be discarded without needing to implement flag operators and extra ancilla qubits. Implementation of the discarding part of the pooling process will therefore be dependent on the exact requirements of the model, although in the worst-case scenario resorting to using F_{FLAG} operators, as described above, to remove specific states would succeed in reducing the image dimensionality.

Appendix E Input Skip Connections Only ResNet

In this section we shall discuss a less general but more qubit efficient implementation of Quantum ResNet where the skipped connection is not between each layer, but only between the input and every other layer in the circuit (until immediately before the final layer).

Theorem 5 (Input Skip Only Quantum ResNet) *It is possible to probabilistically implement a quantum ResNet that only includes skipped connections between the input and every other layer by utilising the LCU method within a quantum variational model. In this context, the implementation of a Quantum Native ResNet for L layers is defined as the implementation of the operator*

$$R_{\text{RES},L}|\phi(\mathbf{x})\rangle = \frac{1}{\Omega'} \sum_{f=1}^L \prod_{l=f}^L |\gamma_f|^2 W_l(\boldsymbol{\theta}_l) |\phi(\mathbf{x})\rangle,$$

where $W_l(\boldsymbol{\theta}_l)$ corresponds to a unitary variational gate implemented in layer l and Ω' is a normalisation constant. The coefficients γ_f correspond to the desired weighting contribution for each layer and can be freely adjusted subject to the requirement that $\sum_f |\gamma_f|^2 = 1$.

Proof The preparation operator can be implemented on k ancilla qubits as a unitary operator

$$P_{\text{PREP}} = \sum_{f=1}^L \gamma_f |b_f\rangle \langle b_1| + \sum_{j=2}^L \sum_{f=1}^L \delta_{jf} |b_f\rangle \langle b_j|, \quad (\text{E31})$$

where the states $\{|b_f\rangle\}_{f \in [1, 2^k]} \in (\mathbb{C}^2)^{\otimes k}$ are basis states of the 2^k dimensional Hilbert space for the k qubit ancilla register denoted by $\mathcal{H} = (\mathbb{C}^2)^{\otimes k}$. This is usually taken to be the computational basis with $|b_1\rangle \equiv |0\rangle^{\otimes k}$. We are only concerned with the $\langle b_1|$ term, as that operator is only applied to $|b_1\rangle$ such that

$$P_{\text{PREP}}|b_1\rangle = \sum_{f=1}^L \gamma_f |b_f\rangle, \quad (\text{E32})$$

subject to the condition that $\sum_f |\gamma_f|^2 = 1$. Subsequently, the selection operator can be applied as

$$S_{\text{SELECT}}|b_f\rangle|\phi(\mathbf{x})\rangle = |b_f\rangle \left(\prod_{l=f}^L W_l(\boldsymbol{\theta}_l) |\phi(\mathbf{x})\rangle \right), \quad (\text{E33})$$

where $\prod_{l=f}^L W_l(\boldsymbol{\theta}_l)$ is a product of unitary operators $W_l(\boldsymbol{\theta}_l)$ and hence clearly implementable on a quantum circuit. Applying the LCU framework we can see that

$$S_{\text{SELECT}} P_{\text{PREP}} |b_1\rangle |\phi(\mathbf{x})\rangle$$

$$= \sum_{f=1}^L \gamma_f |b_f\rangle \left(\prod_{l=f}^M W_l(\boldsymbol{\theta}_l) |\phi(\mathbf{x})\rangle \right). \quad (\text{E34})$$

We can apply the conjugate preparation operator which in general can be written as

$$(P_{\text{PREP}})^\dagger = \sum_{f=1}^L \gamma_f^* |b_1\rangle \langle b_f| + \sum_{j=2}^L \sum_{f=1}^L \delta_{jf}^* |b_j\rangle \langle b_f|, \quad (\text{E35})$$

to find that

$$\begin{aligned} & P_{\text{PREP}}^\dagger S_{\text{SELECT}} P_{\text{PREP}} |b_1\rangle |\phi(\mathbf{x})\rangle \\ &= \sum_{f=1}^L \prod_{l=f}^L |\gamma_f|^2 |b_1\rangle W_l(\boldsymbol{\theta}_l) |\phi(\mathbf{x})\rangle + \sum_{j=2}^L |b_j\rangle (\dots). \end{aligned} \quad (\text{E36})$$

The next step is to measure the ancilla qubits and discard results when the ancilla is not in the $|b_1\rangle$ state, hence we can ignore terms $|b_j\rangle$ for $j \geq 2$. The probability π_S of measuring the ancillas in the $|b_1\rangle$ state corresponds to

$$\pi_S = \left| \sum_{f=1}^L \prod_{l=f}^L |\gamma_f|^2 W_l(\boldsymbol{\theta}_l) |\phi(\mathbf{x})\rangle \right|^2, \quad (\text{E37})$$

and will hence be dependent on the architecture and initial data encoding. Requiring the ancillas to be in the $|b_1\rangle$ state we see that

$$\begin{aligned} & \langle b_1 | P_{\text{PREP}}^\dagger S_{\text{SELECT}} P_{\text{PREP}} |b_1\rangle |\phi(\mathbf{x})\rangle \\ &= \frac{1}{\Omega'} \sum_{f=1}^L \prod_{l=f}^L |\gamma_f|^2 W_l(\boldsymbol{\theta}_l) |\phi(\mathbf{x})\rangle, \end{aligned} \quad (\text{E38})$$

where $\Omega' = \sqrt{\pi_S}$, as required. \square

This LCU method will successfully prepare the desired residual network. Hence we have shown that VQC models can be built with skipped connections under the Quantum ResNet framework by utilising the LCU method to implement these non-unitary operations. An example circuit implementation for the four-layer case $L = 4$ is shown in Figure E3. Notably, this method is more qubit efficient requiring $\mathcal{O}(\log(L))$ qubits for L layers, as opposed to $\mathcal{O}(L)$ qubits in the previous case. It also results in a quadratic (in L) number of terms in the final loss function, which means that the absence of barren plateau argument made in the main text can hold as long as $L = \mathcal{O}(\text{poly}(n))$. This is in contrast to the framework in the main text which in general could contain an exponential (in L) amount of terms in the final loss function. Due to the fact that this could exponentially suppress any beneficially scaling terms, the main text implementation would require that $L = \mathcal{O}(\log(n))$ in order to avoid this.

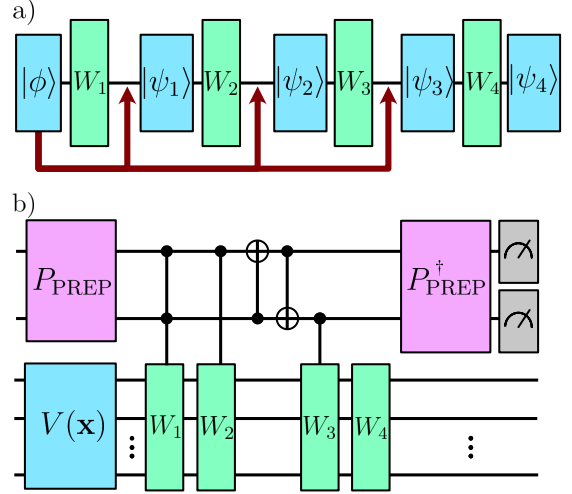


Fig. E3 a) ResNet conceptual illustration in which residual connections are only performed from the input layer to all subsequent layers (stopping before the final layer). b) Circuit implementation of this ResNet using the LCU method, showing the four gate case can be implemented with only two ancilla qubits.

In terms of the probabilistic scaling we see

$$\begin{aligned} \pi_S &= \left| \sum_{f=1}^L \prod_{l=f}^L |\gamma_f|^2 W_l(\boldsymbol{\theta}_l) |\phi(\mathbf{x})\rangle \right|^2 \\ &= \sum_{f,h} |\gamma_h \gamma_f|^2 \left(\langle \phi(x) | \left(\prod_{l=h}^L W_{L-l+h}(\boldsymbol{\theta}_h) \right)^\dagger \right. \\ &\quad \left. \left(\prod_{l=f}^L W_l(\boldsymbol{\theta}_l) \right) | \phi(\mathbf{x}) \rangle \right). \end{aligned} \quad (\text{E39})$$

Hence, the probability of success depends on the encoding state $|\phi(\mathbf{x})\rangle$ and the variational layers, but can also be adjusted through the strength of the residual connection using the γ parameters.

E.1 Two Gate Input Worked Example

In this section we give a brief worked example for the two-layer case of our LCU quantum ResNet with equal weightings.

Consider the encoded quantum state as $|\phi(\mathbf{x})\rangle$ which will be evolved by the first layer of a variational circuit $W_1(\boldsymbol{\theta}_1)$ resulting in the state $|\psi_1(x, \boldsymbol{\theta}_1)\rangle = W_1(\boldsymbol{\theta}_1) |\phi(\mathbf{x})\rangle$.

If we wish to introduce a Quantum ResNet type skipped connection between the input to the first layer then one realisation of this would be implementing the

evolution

$$W_2(\boldsymbol{\theta}_2)(|\phi(\mathbf{x})\rangle + |\psi_1(x, \boldsymbol{\theta}_1)\rangle). \quad (\text{E40})$$

In general, this is not a unitary operation. However, the desired ResNet skipped connection can indeed be written as a linear combination of unitary operations

$$|\psi_2(x, \boldsymbol{\theta}_1, \boldsymbol{\theta}_2)\rangle = (W_2(\boldsymbol{\theta}_2) + W_2(\boldsymbol{\theta}_2)W_1(\boldsymbol{\theta}_1))|\phi(\mathbf{x})\rangle. \quad (\text{E41})$$

This can be implemented using the LCU method by defining P_{PREP} equal to the Hadamard gate such that

$$P_{\text{PREP}}|0\rangle = \frac{1}{\sqrt{2}}(|0\rangle + |1\rangle), \quad (\text{E42})$$

and

$$S_{\text{SELECT}}|0\rangle|\phi(\mathbf{x})\rangle = |0\rangle W_2(\boldsymbol{\theta}_2)|\phi(\mathbf{x})\rangle, \quad (\text{E43})$$

$$S_{\text{SELECT}}|1\rangle|\phi(\mathbf{x})\rangle = |1\rangle W_2(\boldsymbol{\theta}_2)W_1(\boldsymbol{\theta}_1)|\phi(\mathbf{x})\rangle. \quad (\text{E44})$$

After applying the P_{PREP} and S_{SELECT} operators and measuring the ancilla qubit to be in the $|0\rangle$ state, then the appropriate $|\psi_2(x, \boldsymbol{\theta}_1, \boldsymbol{\theta}_2)\rangle$ can be prepared. We show this explicitly through each step for clarity starting with the preparation operator

$$P_{\text{PREP}}|0\rangle|\phi(\mathbf{x})\rangle = \frac{1}{\sqrt{2}}(|0\rangle + |1\rangle)|\phi(\mathbf{x})\rangle, \quad (\text{E45})$$

applying the selection operator

$$\begin{aligned} & S_{\text{SELECT}}P_{\text{PREP}}|0\rangle|\phi(\mathbf{x})\rangle \\ &= \frac{1}{\sqrt{2}}\left(|0\rangle W_2(\boldsymbol{\theta}_2)|\phi(\mathbf{x})\rangle + |1\rangle W_2(\boldsymbol{\theta}_2)W_1(\boldsymbol{\theta}_1)|\phi(\mathbf{x})\rangle\right), \end{aligned} \quad (\text{E46})$$

applying the inverse preparation operator, which is a Hadamard gate we find

$$\begin{aligned} & P_{\text{PREP}}^\dagger S_{\text{SELECT}}P_{\text{PREP}}|0\rangle|\phi(\mathbf{x})\rangle \\ &= \frac{1}{2}\left(|0\rangle((W_2(\boldsymbol{\theta}_2) + W_2(\boldsymbol{\theta}_2)W_1(\boldsymbol{\theta}_1))|\phi(\mathbf{x})\rangle \right. \\ &\quad \left. + |1\rangle(W_2(\boldsymbol{\theta}_2) - W_2(\boldsymbol{\theta}_2)W_1(\boldsymbol{\theta}_1))|\phi(\mathbf{x})\rangle\right), \end{aligned} \quad (\text{E47})$$

measuring the ancilla and requiring it to be in the $|0\rangle$ state gives

$$\begin{aligned} & \langle 0|P_{\text{PREP}}^\dagger S_{\text{SELECT}}P_{\text{PREP}}|0\rangle|\phi(\mathbf{x})\rangle \\ &= \frac{1}{\sqrt{\pi_S}}(W_2(\boldsymbol{\theta}_2) + W_2(\boldsymbol{\theta}_2)W_1(\boldsymbol{\theta}_1))|\phi(\mathbf{x})\rangle, \end{aligned} \quad (\text{E48})$$

which is probabilistically prepared with a probability equal to

$$\begin{aligned} \pi_S &= \frac{1}{4}\langle\phi(x)|(2\mathbb{I} + W_1(\boldsymbol{\theta}_1) + W_1^\dagger(\boldsymbol{\theta}_1))|\phi(\mathbf{x})\rangle \\ &= \frac{1}{2}\left(1 + \text{Re}(\langle\phi(x)|W_1(\boldsymbol{\theta}_1)|\phi(\mathbf{x})\rangle)\right). \end{aligned} \quad (\text{E49})$$

Note that the important part of the probability scaling is the real component of $\text{Re}(\langle\phi(x)|W_1(\boldsymbol{\theta}_1)|\phi(\mathbf{x})\rangle)$. In the case that $W_1(\boldsymbol{\theta}_1) = \mathbb{I}$ then success is guaranteed, and in the case $W_1(\boldsymbol{\theta}_1) = -\mathbb{I}$ then success is impossible. For general $W_1(\boldsymbol{\theta}_1)$ matrices and states $|\phi(\mathbf{x})\rangle$ then the success will vary. It may therefore in practice be worth placing restrictions on $W_1(\boldsymbol{\theta}_1)$ to ensure that $\text{Re}(\langle\phi(x)|W_1(\boldsymbol{\theta}_1)|\phi(\mathbf{x})\rangle)$ does not approach too close to -1 resulting in extremely low success probabilities. However, as mentioned in the main text, if the strength of the residual connections are adjusted it can be possible to increase the lower bound. This example used equal strength in the residual connections for simplicity, which corresponds to the worst-case lower bound.

References

- [1] Shor, P.W.: Polynomial-time algorithms for prime factorization and discrete logarithms on a quantum computer. *SIAM Journal on Computing* **26**(5), 1484–1509 (1997). <https://doi.org/10.1137/s0097539795293172>
- [2] Cao, Y., Romero, J., Olson, J.P., Degroote, M., Johnson, P.D., Kieferová, M., Kivlichan, I.D., Menke, T., Peropadre, B., Sawaya, N.P.D., Sim, S., Veis, L., Aspuru-Guzik, A.: Quantum chemistry in the age of quantum computing. *Chemical Reviews* **119**(19), 10856–10915 (2019). <https://doi.org/10.1021/acs.chemrev.8b00803>
- [3] Herman, D., Googin, C., Liu, X., Galda, A., Safro, I., Sun, Y., Pistoia, M., Alexeev, Y.: A Survey of Quantum Computing for Finance (2022). <https://doi.org/10.48550/arXiv.2201.02773>
- [4] Touvron, H., Lavril, T., Izacard, G., Martinet, X., Lachaux, M.-A., Lacroix, T., Rozière, B., Goyal, N., Hambro, E., Azhar, F., Rodriguez, A., Joulin, A., Grave, E., Lample, G.: LLaMA: Open and Efficient Foundation Language Models (2023). <https://doi.org/10.48550/arXiv.2302.13971>
- [5] Chang, H., Zhang, H., Barber, J., Maschinot, A., Lezama, J., Jiang, L., Yang, M.-H., Murphy, K., Freeman, W.T., Rubinstein, M., Li, Y., Krishnan, D.: Muse: Text-To-Image Generation via Masked

- Generative Transformers (2023). <https://doi.org/10.48550/arXiv.2301.00704>
- [6] Frieder, S., Pinchetti, L., Chevalier, A., Griffiths, R.-R., Salvatori, T., Lukasiewicz, T., Petersen, P.C., Berner, J.: Mathematical Capabilities of ChatGPT (2023). <https://doi.org/10.48550/arXiv.2301.13867>
- [7] Abbas, A., Sutter, D., Zoufal, C., Lucchi, A., Figalli, A., Woerner, S.: The power of quantum neural networks. *Nature Computational Science* **1**(6), 403–409 (2021). <https://doi.org/10.1038/s43588-021-00084-1>
- [8] Beer, K., Bondarenko, D., Farrelly, T., Osborne, T.J., Salzmann, R., Scheiermann, D., Wolf, R.: Training deep quantum neural networks. *Nature Communications* **11**(1) (2020). <https://doi.org/10.1038/s41467-020-14454-2>
- [9] Andrew Childs, N.W.: Hamiltonian simulation using linear combinations of unitary operations. *Quantum Information and Computation* **12**(11, 12) (2012). <https://doi.org/10.26421/qic12.11-12>
- [10] Berry, D.W., Childs, A.M., Cleve, R., Kothari, R., Somma, R.D.: Simulating hamiltonian dynamics with a truncated taylor series. *Physical Review Letters* **114**(9) (2015). <https://doi.org/10.1103/physrevlett.114.090502>
- [11] He, K., Zhang, X., Ren, S., Sun, J.: Deep Residual Learning for Image Recognition (2015). <https://doi.org/10.48550/arXiv.1512.03385>
- [12] Marion, P., Fermanian, A., Biau, G., Vert, J.-P.: Scaling ResNets in the Large-depth Regime (2022). <https://doi.org/10.48550/arXiv.2206.06929>
- [13] Rawat, W., Wang, Z.: Deep Convolutional Neural Networks for Image Classification: A Comprehensive Review. *Neural Computation* **29**(9), 2352–2449 (2017). https://doi.org/10.1162/neco_a.00990
- [14] Sharma, N., Jain, V., Mishra, A.: An analysis of convolutional neural networks for image classification. *Procedia Computer Science* **132**, 377–384 (2018). <https://doi.org/10.1016/j.procs.2018.05.198>
- [15] Al-Saffar, A.A.M., Tao, H., Talab, M.A.: Review of deep convolution neural network in image classification. In: 2017 International Conference on Radar, Antenna, Microwave, Electronics, and Telecommunications (ICRAMET), pp. 26–31 (2017). <https://doi.org/10.1109/ICRAMET.2017.8253139>
- [16] Deng, L.: The mnist database of handwritten digit images for machine learning research. *IEEE Signal Processing Magazine* **29**(6), 141–142 (2012). <https://doi.org/10.1109/MSP.2012.2211477>
- [17] Huang, H.-Y., Broughton, M., Mohseni, M., Babbush, R., Boixo, S., Neven, H., McClean, J.R.: Power of data in quantum machine learning. *Nature Communications* **12**(1), 2631 (2021). <https://doi.org/10.1038/s41467-021-22539-9>
- [18] Heredge, J., Hill, C., Hollenberg, L., Sevier, M.: Permutation invariant encodings for quantum machine learning with point cloud data. *Quantum Machine Intelligence* **6**(25) (2024). <https://doi.org/10.1007/s42484-024-00156-1>
- [19] Larocca, M., Thanasilp, S., Wang, S., Sharma, K., Biamonte, J., Coles, P.J., Cincio, L., McClean, J.R., Holmes, Z., Cerezo, M.: A Review of Barren Plateaus in Variational Quantum Computing (2024). <https://doi.org/10.48550/arXiv.2405.00781>
- [20] Hassan, E., Hossain, M.S., Saber, A., Elmougy, S., Ghoneim, A., Muhammad, G.: A quantum convolutional network and resnet (50)-based classification architecture for the mnist medical dataset. *Biomedical Signal Processing and Control* **87**, 105560 (2024). <https://doi.org/10.1016/j.bspc.2023.105560>
- [21] Saginalieva, A., Kordzanganeh, M., Kurkin, A., Melnikov, A., Kuhmistrov, D., Perelshtein, M., Melnikov, A., Skolik, A., Dollen, D.V.: Hybrid quantum resnet for car classification and its hyperparameter optimization. *Quantum Machine Intelligence* **5**(2) (2023). <https://doi.org/10.1007/s42484-023-00123-2>
- [22] Zaman, K., Ahmed, T., Hanif, M.A., Marchisio, A., Shafique, M.: A Comparative Analysis of Hybrid-Quantum Classical Neural Networks (2024). <https://doi.org/10.48550/arXiv.2402.10540>
- [23] Kashif, M., Al-Kuwari, S.: Resqnets: a residual approach for mitigating barren plateaus in quantum neural networks. *EPJ Quantum Technology* **11**(1) (2024). <https://doi.org/10.1140/epjqt/>

s40507-023-00216-8

- [24] Crognalotti, G., Grossi, M., Vallecorsa, S., Bassi, A.: QResNet: a variational entanglement skipping algorithm. https://indico.cern.ch/event/1288979/contributions/5654644/attachments/2756066/4798864/QTML23_QResNet.pdf
- [25] Cong, I., Choi, S., Lukin, M.D.: Quantum convolutional neural networks. *Nature Physics* **15**(12), 1273–1278 (2019). <https://doi.org/10.1038/s41567-019-0648-8>
- [26] Umeano, C., Paine, A.E., Elfving, V.E., Kyriienko, O.: What can we learn from quantum convolutional neural networks? (2023). <https://doi.org/10.48550/arXiv.2308.16664>
- [27] Hur, T., Kim, L., Park, D.K.: Quantum convolutional neural network for classical data classification. *Quantum Machine Intelligence* **4**(1) (2022). <https://doi.org/10.1007/s42484-021-00061-x>
- [28] Li, Y., Zhou, R.-G., Xu, R., Luo, J., Hu, W.: A quantum deep convolutional neural network for image recognition. *Quantum Science and Technology* **5**(4), 044003 (2020). <https://doi.org/10.1088/2058-9565/ab9f93>
- [29] Pesah, A., Cerezo, M., Wang, S., Volkoff, T., Sornborger, A.T., Coles, P.J.: Absence of barren plateaus in quantum convolutional neural networks. *Physical Review X* **11**(4) (2021). <https://doi.org/10.1103/physrevx.11.041011>
- [30] Liu, J., Lim, K.H., Wood, K.L., Huang, W., Guo, C., Huang, H.-L.: Hybrid quantum-classical convolutional neural networks. *Science China Physics, Mechanics and Astronomy* **64**(9) (2021). <https://doi.org/10.1007/s11433-021-1734-3>
- [31] Kübler, J.M., Buchholz, S., Schölkopf, B.: The inductive bias of quantum kernels (2021). <https://doi.org/10.48550/arxiv.2106.03747>
- [32] Bowles, J., Wright, V.J., Farkas, M., Killoran, N., Schuld, M.: Contextuality and inductive bias in quantum machine learning (2023). <https://doi.org/10.48550/arXiv.2302.01365>
- [33] Meyer, J.J., Mularski, M., Gil-Fuster, E., Mele, A.A., Arzani, F., Wilms, A., Eisert, J.: Exploiting symmetry in variational quantum machine learning. arXiv (2022). <https://doi.org/10.48550/arxiv.2205.06217>
- [34] Nguyen, Q.T., Schatzki, L., Braccia, P., Ragone, M., Coles, P.J., Sauvage, F., Larocca, M., Cerezo, M.: Theory for Equivariant Quantum Neural Networks. arXiv (2022). <https://doi.org/10.48550/arxiv.2210.08566>
- [35] West, M.T., Heredge, J., Seviar, M., Usman, M.: Provably Trainable Rotationally Equivariant Quantum Machine Learning (2024). <https://arxiv.org/abs/2311.05873>
- [36] Schatzki, L., Larocca, M., Nguyen, Q.T., Sauvage, F., Cerezo, M.: Theoretical guarantees for permutation-equivariant quantum neural networks. *npj Quantum Information* **10**(1) (2024). <https://doi.org/10.1038/s41534-024-00804-1>
- [37] Tüysüz, C., Chang, S.Y., Demidik, M., Jansen, K., Vallecorsa, S., Grossi, M.: Symmetry breaking in geometric quantum machine learning in the presence of noise (2024). <https://doi.org/10.48550/arXiv.2401.10293>
- [38] Buzek, V., Hillery, M.: Optimal manipulations with qubits: Universal quantum entanglers. *Physical Review A* **62**(2), 022303 (2000). <https://doi.org/10.1103/PhysRevA.62.022303>
- [39] Barenco, A., Berthiaume, A., Deutsch, D., Ekert, A., Jozsa, R., Macchiavello, C.: Stabilisation of Quantum Computations by Symmetrisation. arXiv (1996). <https://doi.org/10.48550/arxiv.quant-ph/9604028>
- [40] Li, Z., Nagano, L., Terashi, K.: Enforcing exact permutation and rotational symmetries in the application of quantum neural network on point cloud datasets (2024). <https://doi.org/10.48550/arXiv.2405.11150>
- [41] Guala, D., Soni, J., Arrazola, J.M.: PennyLane Tutorial : Linear combination of unitaries and block encodings. https://pennylane.ai/qml/demos/tutorial_lcu_blockencoding/ Accessed:24/05/2024
- [42] Camps, D., Lin, L., Beeumen, R.V., Yang, C.: Explicit Quantum Circuits for Block Encodings of Certain Sparse Matrices (2023). <https://doi.org/10.48550/arXiv.2203.10236>
- [43] Larocca, M., Sauvage, F., Sbahi, F.M., Verdon, G., Coles, P.J., Cerezo, M.: Group-invariant quantum machine learning. *PRX Quantum* **3**(3) (2022). <https://doi.org/10.1103/prxquantum.3.030341>
- [44] Wiersema, R., Kökcü, E., Kemper, A.F., Bakalov,

- B.N.: Classification of dynamical Lie algebras for translation-invariant 2-local spin systems in one dimension (2023). <https://doi.org/10.48550/arXiv.2309.05690>
- [45] Diaz, N.L., García-Martín, D., Kazi, S., Larocca, M., Cerezo, M.: Showcasing a Barren Plateau Theory Beyond the Dynamical Lie Algebra (2023). <https://doi.org/10.48550/arXiv.2310.11505>
- [46] Cerezo, M., Larocca, M., García-Martín, D., Diaz, N.L., Braccia, P., Fontana, E., Rudolph, M.S., Bermejo, P., Ijaz, A., Thanasilp, S., Anschuetz, E.R., Holmes, Z.: Does provable absence of barren plateaus imply classical simulability? Or, why we need to rethink variational quantum computing (2023). <https://arxiv.org/abs/2312.09121>
- [47] Fontana, E., Herman, D., Chakrabarti, S., Kumar, N., Yalovetzky, R., Heredge, J., Sureshbabu, S.H., Pistoia, M.: The Adjoint Is All You Need: Characterizing Barren Plateaus in Quantum Ansätze (2023). <https://arxiv.org/abs/2309.07902>
- [48] Ragone, M., Bakalov, B.N., Sauvage, F., Kemper, A.F., Marrero, C.O., Larocca, M., Cerezo, M.: A Unified Theory of Barren Plateaus for Deep Parametrized Quantum Circuits (2023). <https://arxiv.org/abs/2309.09342>
- [49] Goh, M.L., Larocca, M., Cincio, L., Cerezo, M., Sauvage, F.: Lie-algebraic classical simulations for variational quantum computing (2023). <https://doi.org/10.48550/arXiv.2308.01432>
- [50] Heredge, J., Kumar, N., Herman, D., Chakrabarti, S., Yalovetzky, R., Sureshbabu, S.H., Li, C., Pistoia, M.: Prospects of Privacy Advantage in Quantum Machine Learning (2024). <https://doi.org/10.48550/arXiv.2405.08801>
- [51] Yu, C., Hung, P.-H., Hong, J.-H., Chiang, H.-Y.: Efficient max pooling architecture with zero-padding for convolutional neural networks. 2023 IEEE 12th Global Conference on Consumer Electronics (GCCE), 747–748 (2023). <https://doi.org/10.1109/GCCE59613.2023.10315268>
- [52] Vedral, V., Barenco, A., Ekert, A.: Quantum networks for elementary arithmetic operations. *Physical Review A* **54**(1), 147–153 (1996). <https://doi.org/10.1103/physreva.54.147>
- [53] Galanis, N.I., Vafiadis, P., Mirzaev, K.-G., Papakostas, G.A.: Convolutional neural networks: A roundup and benchmark of their pooling layer variants. *Algorithms* **15**, 391 (2022). <https://doi.org/10.3390/a15110391>
- [54] Gholamalinezhad, H., Khosravi, H.: Pooling Methods in Deep Neural Networks, a Review (2020). <https://doi.org/10.1016/j.isci.2021.103582>
- [55] Zafar, A., Aamir, M., Mohd Nawi, N., Arshad, A., Riaz, S., Alruban, A., Dutta, A., Alaybani, S.: A comparison of pooling methods for convolutional neural networks. *Applied Sciences* **12**, 8643 (2022). <https://doi.org/10.3390/app12178643>
- [56] West, M.T., Erfani, S.M., Leckie, C., Sevier, M., Hollenberg, L.C.L., Usman, M.: Benchmarking adversarially robust quantum machine learning at scale. *Phys. Rev. Res.* **5**, 023186 (2023). <https://doi.org/10.1103/PhysRevResearch.5.023186>
- [57] West, M.T., Nakhil, A.C., Heredge, J., Creevey, F.M., Hollenberg, L.C., Sevier, M., Usman, M.: Drastic circuit depth reductions with preserved adversarial robustness by approximate encoding for quantum machine learning. arXiv preprint arXiv:2309.09424 (2023). <https://doi.org/10.48550/arXiv.2309.09424>
- [58] Dowling, N., West, M.T., Southwell, A., Nakhil, A.C., Sevier, M., Usman, M., Modi, K.: Adversarial robustness guarantees for quantum classifiers. arXiv preprint arXiv:2405.10360 (2024). <https://doi.org/10.48550/arXiv.2405.10360>
- [59] Fulton, W., Harris, J.W.: Representation Theory: A First Course (1991). <https://api.semanticscholar.org/CorpusID:118744956>
- [60] Ragone, M., Braccia, P., Nguyen, Q.T., Schatzki, L., Coles, P.J., Sauvage, F., Larocca, M., Cerezo, M.: Representation Theory for Geometric Quantum Machine Learning (2023). <https://doi.org/10.48550/arXiv.2210.07980>
- [61] Maschke, H.: Ueber den arithmetischen Charakter der Coefficienten der Substitutionen endlicher linearer Substitutionsgruppen. *Mathematische Annalen* **50**(4), 492–498 (1898). <https://doi.org/10.1007/BF01444297>
- [62] Hall, B.C.: Lie Groups, Lie Algebras, and Representations: An Elementary Introduction. Graduate Texts in Mathematics, vol. 222. Springer, Cham (2015). <https://doi.org/10.1007/978-3-319-13467-3>

- [63] Jean-Pierre, S.: Linear Representations of Finite Groups. <https://link.springer.com/book/10.1007/978-1-4684-9458-7>
- [64] Huppert, B.: Character Theory of Finite Groups. De Gruyter, Berlin, New York (1998). <https://doi.org/10.1515/9783110809237>
- [65] Deitmar, A.: A first course in harmonic analysis (2002). https://doi.org/10.1007/978-1-4757-3834-6_10
- [66] Raut, G., Patole, A.: End-to-End 3D Object Detection using LiDAR Point Cloud (2023). <https://doi.org/10.48550/arXiv.2312.15377>
- [67] Kirby, W.M., Strauch, F.W.: A practical quantum algorithm for the schur transform. Quantum Information and Computation **18**(9, 10), 721–742 (2018). <https://doi.org/10.26421/qic18.9-10-1>
- [68] Kirby, W.M.: A Practical Quantum Schur Transform. BA Thesis. <https://doi.org/https://static1.squarespace.com/static/5a1461108fd4d28cad8dae2c/t/5af30798575d1f7240339f36/1525876638766/William+M+Kirby+Thesis+v2.pdf>. Accessed: 24/05/2024
- [69] Anschuetz, E.R., Bauer, A., Kiani, B.T., Lloyd, S.: Efficient classical algorithms for simulating symmetric quantum systems. Quantum **7**, 1189 (2023). <https://doi.org/10.22331/q-2023-11-28-1189>
- [70] Abraham, H., AduOffei, Agarwal, R., Akhalwaya, I.Y., Aleksandrowicz, G., et al Ćepulkovskis: Qiskit: An Open-source Framework for Quantum Computing (2019). <https://doi.org/10.5281/zenodo.2562110>
- [71] Havlíček, V., Córcoles, A.D., Temme, K., Harrow, A.W., Kandala, A., Chow, J.M., Gambetta, J.M.: Supervised learning with quantum-enhanced feature spaces. Nature **567**(7747), 209–212 (2019). <https://doi.org/10.1038/s41586-019-0980-2>
- [72] Heredge, J., Hill, C., Hollenberg, L., Seviar, M.: Quantum support vector machines for continuum suppression in b meson decays. Computing and Software for Big Science **5** (2021). <https://doi.org/10.1007/s41781-021-00075-x>
- [73] Bacon, D., Chuang, I.L., Harrow, A.W.: Efficient Quantum Circuits for Schur and Clebsch-Gordan Transforms. Physical Review Letters **97**(17), 170502 (2006). <https://doi.org/10.1103/PhysRevLett.97.170502>
- [74] Krovi, H.: An efficient high dimensional quantum Schur transform. Quantum **3**, 122 (2019). <https://doi.org/10.22331/q-2019-02-14-122>